



Mercury speciation in a tropical soil association; Consequence of gold mining on Hg distribution in French Guiana

Stéphane Guédron, Sylvain Grangeon, Bruno Lanson, Michel Grimaldi

► To cite this version:

Stéphane Guédron, Sylvain Grangeon, Bruno Lanson, Michel Grimaldi. Mercury speciation in a tropical soil association; Consequence of gold mining on Hg distribution in French Guiana. *Geoderma*, 2009, 153 (issues 3-4), pp.331-346. 10.1016/j.geoderma.2009.08.017 . insu-00424551

HAL Id: insu-00424551

<https://insu.hal.science/insu-00424551>

Submitted on 16 Oct 2009

HAL is a multi-disciplinary open access archive for the deposit and dissemination of scientific research documents, whether they are published or not. The documents may come from teaching and research institutions in France or abroad, or from public or private research centers.

L'archive ouverte pluridisciplinaire **HAL**, est destinée au dépôt et à la diffusion de documents scientifiques de niveau recherche, publiés ou non, émanant des établissements d'enseignement et de recherche français ou étrangers, des laboratoires publics ou privés.

**Mercury speciation in a tropical soil association;
Consequence of gold mining on Hg distribution in French Guiana.**

Stéphane GUEDRON^{a,*}, Sylvain GRANGEON^b, Bruno LANSON^b, and Michel GRIMALDI^c.

^a Environmental Geochemistry Group - LGIT, Observatory of Earth and Planetary Science (OSUG), University of Grenoble / CNRS - Maison des Géosciences, 1381, rue de la Piscine - Domaine Universitaire - 38400 Saint-Martin-D'Hères, France.

^b Mineralogy & Environments - LGCA, Observatory of Earth and Planetary Science (OSUG), University of Grenoble / CNRS - Maison des Géosciences, 1381, rue de la Piscine - Domaine Universitaire - 38400 Saint-Martin-D'Hères, France.

^c UMR Bioemco- Biogéochimie et Ecologie des Milieux Continentaux, UMR211, Institut de Recherche pour le Développement, 32 avenue Henri Varagnat, 93143 Bondy, France.

* Corresponding author – Present address: Institut F.A.-Forel, route de Suisse 10, CP416, 1290 Versoix, Switzerland.

E-mail: stephane.guedron@unige.ch

Tel : +41-223-790-311

Fax : +41-223-790-329

Abstract.

Mercury (Hg) speciation was compared in French Guiana pristine soils and in Hg contaminated soils impacted by former (~1950's) gold-mining activities which used Hg for gold amalgamation. Four selective extractions were performed on soil samples to assess the fraction of Hg present as Hg(II) and bond to organic matter (extracted by NH_4OH and KOH), to amorphous iron oxides (ascorbate) and to soil components other than refractory minerals (HCl/HNO_3). In addition, pyrolysis was used to quantify the content of elemental Hg in contaminated soils. X-ray diffraction (XRD) and X-ray fluorescence micro-mapping (μXRF) were used in combination to selective extractions to assess the nature of targeted components, the possible overlaps between the different extraction procedures and the spatial correlation between Si, K, Fe, Au and Hg.

In soil profiles from pristine toposequences, Hg concentrations ($0.01\text{--}0.49\ \mu\text{g.g}^{-1}$) decreased with increasing depth in soil matrix. Hg concentrations also decreased from ferralsols to acrisols and further to gleysols. In pristine soil matrix, Hg was mainly associated to the clay size fraction ($< 2\ \mu\text{m}$) which was mainly constituted of amorphous and crystalline Fe oxides (Al-substituted goethite and hematite), gibbsite and fine organic matter (OM), whose relative abundances vary along the soil association. Total Hg concentration was positively correlated with sulfurs and organic carbon suggesting the association of Hg with OM sulfur-bearing functional groups. Gleysols were depleted in Hg because of the prevailing reducing conditions that lead to the dissolution of iron oxides. In the same soil profiles, Hg concentrations in ferruginous nodules, which make up most of the soil coarse fraction ($> 2\ \text{mm}$), were similar to those reported in the pristine soil matrix. These nodules mainly contained Al-substituted hematite and goethite and were especially abundant upslope in

ferralsols and Acrisols. Gold-mined gleysols were strongly disorganized by former activities as neither the original structure nor the texture was preserved. Soil granulometry was dominated by gravels, sands and silts. Hg concentrations ($0.09\text{--}9.22\ \mu\text{g}\cdot\text{g}^{-1}$) largely exceeded those in pristine soils. μXRF allowed the identification of Au-amalgamated Hg and of elemental Hg droplets. Pyrolysis confirmed Hg to be mainly present in its elemental form in contaminated soils. Selective extractions showed additional minor contributions of Hg(II) associated to OM, and to Al or Fe oxides.

The combination of selective extractions with XRD and μXRF data showed that extraction efficiency is strongly dependent on the soil type, and that this efficiency needs to be determined on a soil-by-soil basis for Hg speciation studies. KOH extraction was especially delicate as crystalline and amorphous oxides were extracted together with organic matter.

Key-words: Mercury, Tropical soils, French Guiana, gold-mining, XRD, selective extraction, speciation.

1. Introduction

Tropical soils from the Amazonian basin are known to have accumulated atmospheric Hg over millions of years, thus inducing geochemical backgrounds higher than those reported in boreal and temperate climate soils (Carmouze et al., 2001). In addition, past and current gold mining activities, which represent the main contribution to anthropogenic emissions (Lacerda, 1997; Roulet et al., 1998; Guedron et al., 2006), contribute to increase further the total Hg concentrations in these soils. Small-scale mining activities have increased significantly during the worldwide gold rush, created by the gold price increase in the 1980's. UNIDO (United Nations Industrial Development Organization) estimates that in 2004 10 to 15 million people were working in small-scale gold mines releasing 650-1000 tons of Hg annually (Veiga and Baker, 2004). In addition to this major atmospheric emission, gold mining activities release large amounts of Hg-rich particles into hydrosystems where methylmercury (MMHg) production has been clearly identified in anoxic and suboxic areas (Benoit et al., 2003; Coquery et al., 2003). In turn, MMHg accumulation along the aquatic food chains is a threat to Amerindian populations whose diet relies mainly on fish (Lebel et al., 1996; Frery et al., 2001; Barbosa et al., 2003). To assess Hg mobility and its availability to methylating microorganisms, it is thus crucial to determine how Hg is bond to soil particles.

The retention capacity of tropical soils varies as a function of soil components which depends on soil types and horizons (Charlet and Sposito, 1987; Charlet and Sposito, 1989; Fontes and Gomes, 2003). In particular, the relative proportions of soil components responsible for Hg retention [clay minerals, Fe-, Al-, and Mn-(oxyhydr)oxides, organic matter] vary with the geochemical conditions which in turn

depend on the topographic position along the soil association (Boulet et al., 1993; do Valle et al., 2005; Fritsch et al., 2005; Fritsch et al., 2006).

Hg has a high affinity for soil organic matter, especially for reduced sulfur groups such as thiol ligands (Schuster, 1991; Skyllberg et al., 2000; Khwaja et al., 2006; Skyllberg et al., 2006). High Hg levels can also be associated to Fe-(oxyhydr)oxides. In particular, amorphous or poorly crystalline oxides are known as sinks for metal contaminants owing to their large surface area and/or microporous structure (Trivedi and Axe, 2001). Ferruginous nodules, formed during the lateritic weathering process, also contain elevated Hg contents (Roulet and Lucotte, 1995; Roulet et al., 1998; De Oliveira et al., 2001; Brabo et al., 2003).

Solid-phase chemical speciation has been widely used on sediment samples to decipher metal distribution in contaminated systems (Wallschlager et al., 1998; Rodriguez Martin-Doimeadios et al., 2000; Beldowski and Pempkowiak, 2003; Bloom et al., 2003; Boszke et al., 2006). Most of the recent studies of Hg speciation in natural or contaminated sediments, soils and tailings used sequential extraction procedure (SEP) or Hg pyrolysis procedure following published recommendations (Eagenhouse et al., 1978; Di Giulio and Ryan, 1987; Biester and Scholz, 1997; Bloom et al., 2003). While some studies strictly follow the described SEP (Sanchez et al., 2005; Beldowski and Pempkowiak, 2007), many authors adapt it to the studied matrix. Each extraction step of the SEPs for soils and sediments is critical, as it is challenging to obtain an adequate recovery by preventing losses, contamination or speciation changes, and limiting the interferences (Leermakers et al., 2005).

In the present study, the speciation of Hg among soil components was determined in soil profiles along pristine soil toposequences and in soils contaminated with Hg by former gold mining in a French Guiana watershed.

Separate selective extractions were used to quantify Hg distribution between soil carrier phases, in order to avoid cumulative errors intrinsic to SEPs. In addition, the combination of X-ray diffraction (XRD) and chemical analysis allowed the identification of the extracted phases and of possible overlaps between selective extractions (cross recoveries). Intrinsic limitations of the selective extraction procedure are discussed in the light of these results.

2. Materials and methods.

2.1. Research areas

The former gold mine flat is located in French Guiana (Fig. 1) on the Combat Creek watershed (52°23'W, 4°35'N), a small catchment of ~1 km² covered by tropical rain forest. Except for the two hilltops and for the lowland, the relief is characterized by steep slopes (15-30%). The climate is tropical humid, with an annual average rainfall of ~4000 mm (Barret, 2004).

The Combat Creek watershed is located on the 'Amina series' of the Guiana Proterozoic shield consisting primarily of darkschist and thin sandstones (Milési et al., 1995). Large gravel deposits from ancient rivers contain large amounts of gold, resulting from the weathering of auriferous quartz veins from the Proterozoic shield (Milési et al., 1995).

Soil distribution within the Combat Creek watershed is typical of French Guiana and is related to soil position along the slopes (Boulet et al., 1979; Grimaldi et al., 2001; Guedron et al., 2006). Ferralsols dominate upslope (Deckers et al., 1998), having typically a high clay (< 2 µm size fraction) content and a micro-aggregated structure extending over 1 m depth, which allows a good vertical water drainage (Guehl, 1984). Ferruginous nodules are present throughout the entire ferralsol

profiles. Halfway down the slopes, ferralsols steadily evolves to Acrisols, a massive alteritic horizon with a high content of fine silts at shallow depth (< 1 m). During rainfalls, a perched aquifer forms on the slope above this massive alteritic horizon. Following rainfalls, the aquifer is evacuated laterally, exporting preferentially clay-size particles and dissolution products (Molicova et al., 1997; Grimaldi et al., 2004). Downslope, the soils become hydromorphic, with dominant sands. A permanent aquifer is present and slowly drained by the river, thus imposing reducing conditions. Whatever the soil type, field observations have shown that quartz, kaolinite, and Fe-Al-(oxyhydr)oxides dominate mineralogy, quartz being the sole remnant from the primary rock-forming minerals. In the massive alteritic horizon, a few muscovite crystals were also observed. Soil pH ranged from 4.2 to 4.9. The upper part of the studied watershed (ferralsols and Acrisols) was considered to be pristine based on the soil structure and texture.

In the lowland, ancient 'Long Tom' sluices and gold-bearing gravel heaps attest of former gold mining activities dated from the early 1950's. These activities involved the removal of fine particles with water, in order to concentrate heavier gold-rich particles. Soils are thus strongly disorganized, and neither original structure nor texture is preserved. Present day soil granulometry reflects the former activity as gravels, sands and silts are dominant, while the clay-size fraction is almost absent. Hg droplets were also observed in these gold-mined gleysols during a prospective "panning" campaign. These soils can be described as disorganized gleysols according to their present geochemical characteristics.

2.2. Sampling collection and analysis

2.2.1 Soil collection

Three toposequences were sampled in the pristine part of the watershed, (i) the first in the upper part of the basin, (ii) the second on the west (mountain) side and (iii) the third next to the outlet of the basin (Fig. 1). Toposequences II and III reached the gold-mined flats (profiles II-0 and III-0 in Fig. 1).

Thirteen profiles were collected in the former gold-mined flat. SL0 to SL9 profiles were mesh-sampled over a restricted 250 m² area in the flat zone (Fig. 1). G5 profile was sampled on a gravel heap. Soil profiles were sampled systematically every 10 or 20 cm, down to 1-2 m depth, using an auger and collected in sterile polyethylene bags.

2.2.2 Soil conditioning, granulometry and chemical analysis

Granulometry was determined with standard sieving and sedimentation procedures (Avery and Bascomb, 1974; Rowell, 1994). Identification of the various fractions was performed according to the Udden-Wentworth classification scheme (Wentworth, 1922), and “gravel”, “sand”, “silt” and “clay” thus refer to particle diameters (x) of $x > 2$ mm, $2\text{ mm} < x < 50\text{ }\mu\text{m}$, $50\text{ }\mu\text{m} < x < 2\text{ }\mu\text{m}$ and $x < 2\text{ }\mu\text{m}$, respectively. Total soil organic carbon ([C]), sulfur ([S]), and nitrogen ([N]) concentrations were determined from the dry combustion of soil sample aliquots crushed and sieved to 63 μm , using a Fisons 1500CHNS auto-analyzer.

Soil samples aliquots used for Hg analysis, selective extractions and XRD analysis were freeze-dried and sieved to $x < 2$ mm. This size fraction was subsequently crushed to $x < 63\text{ }\mu\text{m}$. Ferruginous nodules were crushed also to $x < 63\text{ }\mu\text{m}$ and subsequently freeze-dried. Total Hg concentrations ([HgT]) were

determined by atomic absorption spectrophotometry after dry mineralization and gold amalgamation with an automatic mercury analyzer (Altec, Model AMA 254). All analyses were duplicated. The relative error was routinely $\pm 5\%$ and always under $\pm 10\%$ (Roos-Barracough et al., 2002). Detection limit (defined as three times the standard deviation (SD) of the blank) is $0.005 \mu\text{g g}^{-1}$. Concentrations obtained for repeated analyses of certified reference materials (CRMs) never exceeded the published range of concentration ($0.090 \pm 0.012 \mu\text{g g}^{-1}$ and $0.091 \pm 0.008 \mu\text{g g}^{-1}$ for CRMs 7002, and MESS-3, respectively). Total dissolved Hg concentration $[(\text{HgT})_{\text{D}}]$ were analyzed by cold vapor atomic fluorescence spectrometry (CVAFS) after conversion of all mercury species to Hg^0 (Bloom and Fitzgerald, 1988), using a Tekran[®] instrument (Model 2500). Additional information on the method is available elsewhere (Bloom and Fitzgerald, 1988). $(\text{HgT})_{\text{D}}$ concentrations obtained for repeated analyses of CRMs never exceeded the published range of concentration ($12.6 \pm 1.1 \text{ ng L}^{-1}$ for ORMS-3). The detection limit is 0.05 ng L^{-1} (Bloom and Fitzgerald, 1988).

Dissolved Fe and Al were determined by inductively coupled plasma-atomic emission spectrometry (ICP-AES) using a Perkin-Elmer optima 3300DV. Calibration was performed with using standard solutions for Fe and Al (Fluka[®] 44903 for Fe and Fluka[®] 06155 for Al). Relative analytical errors were estimated for each sample from triplicate measurements and were lower than 10%.

2.3. Selective extraction procedure for Hg and major element analysis

2.3.1 Sample selection

Along soil profiles, samples were selected on the basis of characteristics such as granulometry, C and/or Hg contents, reflecting the textural and structural

variations along soil profiles. In pristine soils, the selection criteria were extreme contents of C, Hg, clay-size fraction, and fine-silt fraction which increased in alterites. In contaminated gleysols from the gold-mined flat, the selection relied mainly on the abundance of the clay- and sand-size fractions, as well as on C and Hg concentrations.

In addition to selected samples, selective extractions were performed for quality assurance/quality controls (QA/QC) on 2 CRMs, namely a light sandy soil (CRM 7002 - Czech Metrological Institute) and a marine sediment (MESS-3 -National Research Council of Canada - Ottawa) and on two natural samples. The latter two samples [acrisol I-1 (0-10 cm), and contaminated gleysol SL6 (30-50 cm)] were chosen as models for the pristine and contaminated parts, respectively, of the watershed. On all samples [HgT] was measured on both the supernatant and the solid residue to assess extraction recovery. In addition, XRD data was systematically collected on solid residues to identify dissolved mineral species.

2.3.2 Selective extraction materials and procedure

Four chemical extractions were chosen to selectively extract the main Hg carrier phases reported in the literature for tropical soils: organic matter, amorphous Fe oxides, and crystalline Fe/Al oxides.

For a given sample, selective extractions were performed on separate aliquots of dry soil (~ 40 mg). All analytical procedures were conducted using ultra clean sample handling to avoid laboratory contamination of low-level sample extracts and a cross-contamination of high-level samples (Cossa and Gobeil, 2000). Specifically, all materials in contact with the samples were previously acid washed (1 week in HNO₃ 20%, 1 week in HCl 10%). All solutions were prepared from reagent grade chemicals and supra-pure acids. Selective extractions were performed under a laminar hood in

8 ml Teflon[®] vessels at a 1:100 solid-to-liquid ratio (Bloom et al., 2003). At the end of the extraction time, samples were centrifuged to 3000 rpm for 20 min. The supernatant was analyzed for major elements. The solid residue was rinsed 3 times with 4 mL MilliQ[®] water to obtain a final volume of ~16 mL, which was subsequently freeze-dried before Hg analysis. The Hg content extracted by a given extraction was calculated as:

$$[\text{Hg}]_{\text{extracted}} (\text{ng g}^{-1}) = ([\text{HgT}] \times M_{\text{sample}} - M_{\text{Hg in residue}}) / M_{\text{sample}} \quad (1)$$

where M_{sample} is the mass of the aliquot used (in g) and $M_{\text{Hg in residue}}$ the mass of Hg measured in the residue (in ng).

To extract Hg bond to fulvic and humic compounds, a sample aliquot was digested in NH_4OH (1M) for 1h (Di Giulio and Ryan, 1987; Rodriguez Martin-Doimeadios et al., 2000; Veiga and Baker, 2004). Another extraction focused on organo-chelated Hg was performed by a 18h KOH digestion (1M) (Bloom et al., 2003). Extraction of Hg bond to amorphous Fe(III) oxide minerals and ferrihydrite was performed by adding ascorbate to a sample aliquot and allowing it to react at room temperature for 24h (Kostka and Luther III, 1994). Finally, extraction of Hg associated to all soil components except refractory minerals (i.e., silicates, primary minerals) was determined after the digestion of soil sample aliquot in a Suprapur HCl/HNO_3 solution (1/9 v/v ratio) for 10h at 70°C (Coquery et al., 1997; Bloom et al., 2003). All species associated to a specific extractant are labeled as follow: $(i)_j$ where i is the element and the subscribe j describes the extractant (i.e., $(i)_{\text{NH}_4\text{OH}}$ for NH_4OH , $(i)_{\text{KOH}}$ for KOH , $(i)_{\text{Asco}}$ for ascorbate and $(i)_{\text{HCl/HNO}_3}$ for HCl/HNO_3) and square brackets, $[i]_j$, are used for calculated concentrations (1). The concentration of Hg related to crystalline and refractory minerals (RC) is calculated as the difference between $[\text{HgT}]$ and ascorbate plus NH_4OH extractions:

$$[\text{Hg}]_{\text{RC}} (\text{ng g}^{-1}) = ([\text{HgT}] \times M_{\text{sample}}) - M_{\text{Hg Asco}} - M_{\text{Hg NH}_4\text{OH}} / M_{\text{sample}} \quad (2)$$

This should be equivalent to a complete HF/HCl/HNO₃ extraction. Similar calculations were made to estimate the fraction of Hg bond to crystalline Fe and Al oxides ([i]_{Cryst}). For this purpose, concentrations obtained after HCl/HNO₃ extraction were considered as related to amorphous and crystalline Fe and Al oxides but not to refractory minerals. Thus, [i]_{Cryst} was calculated as the difference between HCl/HNO₃ and ascorbate extraction :

$$[i]_{\text{Cryst}} (\text{mg g}^{-1}) = ([i]_{\text{HCl/HNO}_3} \times M_{\text{HCl/HNO}_3} - [i]_{\text{Asco}} \times M_{\text{Asco}}) / M_{\text{sample}} \quad (3)$$

A complementary pyrolysis procedure was used to assess the amount of Hg⁰ present in the soils (Biester, 1994; Biester and Scholz, 1997; Bollen et al., 2008). After heating a ~1g sample aliquot for 48 hours at 180°C in a porcelain crucible, the content of Hg⁰ was determined from the difference in Hg concentrations between raw and treated samples.

2.4. Physical methods

2.4.1 X-ray diffraction

X-ray diffraction (XRD) was performed on selected samples [Nodules I-2 (10-20 cm), I-1 (30-40 cm) and I-1 (180-200 cm)] for routine mineralogical identification, but also to identify the minerals targeted by the various selective extractions on CRM 7002, and MESS-3 standards, as well as on samples I-1 (0-10 cm) and SL6 (30-50 cm). For this purpose, XRD patterns were collected on solid residues of the different extractions, and compared to those obtained on the untreated samples.

XRD patterns were recorded on randomly oriented powders using a Bruker D5000 powder diffractometer equipped with a Si(Li) solid-state detector from Baltic Scientific Instruments and CuKα radiation (λ = 1.5418 Å). Intensities were recorded

from 5 to 80°2 θ , using 0.04°2 θ steps, and 40 s counting time per step. Measurements were duplicated on the CRM 7002 set of samples to ensure sampling homogeneity and selective extraction reproducibility (data not shown).

Mineralogical identification and unit-cell refinement

Basic data processing operations (e.g. background removal, diffractogram normalization) and mineralogical identification, based on peak positions and relative intensities, were performed using the Bruker Difract^{plus} EVA software and the ICDD database.

Relative intensities of XRD lines varied between raw and treated samples as the result of specific mineral dissolutions. To overcome the intensity variations due to the amount of measured sample, all XRD patterns were normalized to a selected quartz peak, as quartz was present in all samples and not dissolved by the reagents used. The peak used for normalization was selected so that (i) there is no peak overlap with other minerals and (ii) that its intensity is statistically meaningful. For iron oxides (hematite and goethite) present in Al-rich environments, experimental peak positions may differ significantly from theoretical ones as the result of isomorphic Al-for-Fe substitutions. In such case, theoretical unit-cell parameters of iron oxides were refined using the U-Fit program (Evain, 1992) to assess their Al-contents.

2.4.2 Micro X-ray fluorescence mapping and elemental analysis.

SL6 (30-50 cm) sample was freeze-dried, sieved to 300 μ m and used for elemental mapping focused on Hg, Au, Al, Cl, Fe, Cr, Si, Ti, Mn, Ni, Ca and K. X-ray fluorescence yields (XRF) were measured with an Eagle III μ -XRF spectrometer (Röntgenanalytik Messtechnik GmbH) equipped with a Rh anode and a 40 μ m poly-capillary. XRF was measured for 300 s per point over a 1.28×1.00 mm² surface area. The spectrometer was operated under vacuum at 25 kV and 500 μ A so as to

maximize the fluorescence yield at the Hg L_α edge (9.99 keV) while keeping a statistically significant signal on light elements (down to Al K_α radiation - 1.49 keV). Further details on the method are given elsewhere (Doering et al., 2004).

2.5 Statistical treatment.

Since geochemical data were not normally distributed, the following parameters are reported: mean, standard error on the mean (SEM), median, 25th and 75th percentiles (25th perc. and 75th perc., respectively) and the number of observations (N - Webster, 2001). In addition, non parametric Mann-Whitney rank sum test (*U* test) and Kruskal-Wallis one way analysis of variance on ranks (*H* test) were used to compare two or more than two data sets, respectively. Pearson correlations were applied to compare multiple data set pairs. Correlation coefficient (CC) and P values (P) are reported.

3. Results

3.1 Blanks and CRMs

3.1.1 Mineralogy (QA/QC)

XRD patterns obtained on treated CRM samples indicate that halite was dissolved by all reagents (Supplementary data - Figs E1b. to E1e. and E2b to E2e). For CRM 7002, the chlorite component was partly dissolved by both NH₄OH and KOH. Exception made of halite, the effect of ascorbate was negligible. Most of the minerals identified by XRD were thus only affected by HCl/HNO₃: clinocllore, calcite and dolomite were totally dissolved, and an intensity decrease was observed for hornblende and, to a lesser extent, for kaolinite (Supplementary data – Figs E1e. and E2e.).

3.1.2 Extraction recoveries (QA/QC)

For NH_4OH , KOH and HCl/HNO_3 extractions, summation of M_{Hg} in both the supernatant and the solid residue led to total Hg concentration consistent with those of CRM 7002, MESS-3 and I-1 (10-20cm) sample. Relative error was routinely less than $\pm 10\%$ (Tab. E1). Hg recovery was lower with ascorbate extraction, possibly due to the loss of Hg^0 in the supernatant following Hg^{II} reduction (Battke et al., 2008). Consistent with this hypothesis, additional measurements of $[(\text{Hg})_{\text{D}}]$ in the supernatant confirmed a steady decrease with time at the end of the extraction.

3.2. Pristine soils

3.2.1 Granulometry, chemistry and mineralogy

In the pristine area, the relative proportion of the clay-size fraction ($< 2 \mu\text{m}$) decreased from $\sim 90\%$ in ferralsols to less than 30% in acrisols and gleysols (Fig. 2). Ferruginous nodules made up most of the abundant gravel size fractions ($x > 2 \text{ mm}$) in ferralsols and acrisols, whereas for gleysols vegetal debris prevailed in this size fraction. In the $< 2 \text{ mm}$ fraction, total C and S contents in superficial horizons decreased from ferralsols and acrisols to gleysols while the C/N ratios were similar for all soils, thus indicating an homogeneous mineralization of the fine organic matter (OM - Bravard and Righi, 1991).

Minerals extracted by HCl/HNO_3 in sample I-1 (0-10cm) were identified as Al-substituted iron oxides (goethite and hematite) and gibbsite (Fig. 3). Quartz, anatase, kaolinite, and muscovite being essentially unaffected by the HCl/HNO_3 extraction (Supplementary data – Fig. E3e.).

For HCl/HNO_3 and ascorbate extractions, Fe and Al concentrations were correlated to the content of the clay size fraction (Tab. 1) showing that crystalline and

amorphous Fe and Al oxides were central in this fine fraction. Large Al and Fe concentrations were measured in supernatants following KOH, ascorbate and NH₄OH extractions. XRD confirmed that no crystalline Fe or Al oxides were dissolved by NH₄OH, thus supporting the dissolution of amorphous (or poorly crystalline) Fe and/or Al minerals. In addition, goethite was partially dissolved by ascorbate and hematite by KOH, as indicated by the ~10-20% intensity decrease of their characteristic XRD lines after these chemical extractions (Fig. 3). For all pristine soil samples, partial dissolution of these well-crystallized species is supported by the higher Al and Fe concentrations measured in KOH (median = 52.6% and 12.1% of [Al]_{HCl/HNO₃} and [Fe]_{HCl/HNO₃}) and ascorbate (median = 24.7% and 21.7% of [Al]_{HCl/HNO₃} and [Fe]_{HCl/HNO₃}) extracts compared to NH₄OH extracts (median=9.1% and 3.6% of [Al]_{HCl/HNO₃} and [Fe]_{HCl/HNO₃}) (*H* test, *P* < 0.001).

[Fe]_{HCl/HNO₃}, [Al]_{HCl/HNO₃}, [Fe]_{Asco} and [Al]_{Asco} decreased steadily along the slopes from ferralsols to gleysols (Fig. 4), [Fe]_{Asco} and [Al]_{Asco} being commonly lower than [Fe]_{Cryst} and [Al]_{Cryst} for all profiles (Fig. 4). In ferralsols and acrisols, amorphous Fe and Al oxides were most abundant in the A horizon and in the top 50 cm of the B horizon, where weathering was most intense and granulometry dominated by clays. In the C horizon, the relative proportion of amorphous oxides decreased while well crystallized oxides and residual primary minerals became predominant, more especially in the fine silt size fraction. Al-for-Fe substitutions were identified in goethite (~33 Al mol%) and hematite (~10 Al mol%) from XRD unit-cell determinations and confirmed by the positive correlations between [Fe]_{Cryst} and [Al]_{Cryst} in B and C horizons (Fig. 4 - CC = 0.76; *P* < 0.01). Similar correlation was observed between [Fe]_{Asco} and [Al]_{Asco} (CC = 0.98; *P* < 0.01) for the whole profiles of pristine soils. The better correlation found between [Fe] and [Al] for ascorbate than

for crystalline oxide is suggestively due to an increase in [Al] related to Al extraction from gibbsite and in a lesser extent from kaolinite during HCl/HNO₃ extraction.

3.2.2 Hg in pristine soils

Total mercury concentrations measured in pristine soils matrix (0.01-0.49 µg.g⁻¹ - Fig. 2) were consistent with those recently reported for French Guiana soils (0.09-0.50 µg.g⁻¹ - Richard et al., 2000; Grimaldi et al., 2001; Guedron et al., 2006), the highest concentrations being measured in ferralsols. [HgT] decreased along the slope in acrisols and in gleysols (Fig. 2).

[HgT] were positively correlated with [Hg] extracted by HCl/HNO₃, KOH, NH₄OH and ascorbate (Tab. 1). In turn, [Hg] extracted by the four reagents were positively correlated to the content of the clay-size fraction, [S] and [C]. The clay-size fraction, which is composed of OM (S-groups) and Fe and Al minerals, thus represents the main Hg reservoir (Tab. 1).

In general, [Hg] extracted by all four reagents decreased with depth and from ferralsols to gleysols. However, Figure 5 shows that Hg extraction yields can be separated in two sets: (i) ferralsols and superficial acrisols and (ii) deep acrisol alteritic (C) horizons and gleysols. In both sets, NH₄OH extraction yields were significantly larger than ascorbate ones but followed the same trend. (Hg)_{NH₄OH} and (Hg)_{Asco} extraction yields were highest in superficial horizons of both ferralsols and acrisols and steadily decreased with depth. Only in the upstream profiles I-1 and I-2 (Hg)_{NH₄OH} and (Hg)_{Asco} extraction yields were constant with depth. In gleysols and deep alteritic horizons of acrisols, both (Hg)_{NH₄OH} and (Hg)_{Asco} decreased rapidly with depth, whereas (Hg)_{RC} extraction yields increased strongly with increasing depth. (Hg)_{RC} decreased with increasing depth in the B horizons of ferralsols and acrisols, then increasing steadily in the ferralsol C horizons. (Hg)_{KOH} extraction yields were

highly variable with highest values in ferralsol and Acrisol B horizons. In pristine gleysols (profile II-1), $(\text{Hg})_{\text{KOH}}$ extraction yields increased with increasing depth over the first 50 cm, while decreasing in the C horizon.

3.3 Ferruginous nodules in pristine soils

3.3.1 Chemistry and mineralogy

Ferruginous nodules (> 2 mm) were abundant (mean \pm RSD = $45.8 \pm 28.6\%$ total weight), especially in superficial horizons of the pristine toposequences, their relative abundance decreasing from ferralsols to gleysols. Nodules from samples I-2 (10-20 cm), I-2 (30-40 cm) and I-2 (180-200 cm) contained quartz, Al-substituted hematite and goethite, gibbsite and kaolinite. Figure 6 shows the steady increase of muscovite (Mu), paragonite (Pa), gibbsite (Gb) and rutile (Ru) contents from surface (sample I-2, 10-20 cm) to depth (sample I-2, 180-200 cm - Fig E4). This mineralogical evolution is consistent with chemical data as $[\text{Fe}]_{\text{HCl/HNO}_3}$ and $[\text{Al}]_{\text{HCl/HNO}_3}$ steadily decreased with increasing depth.

Position of the iron oxide peaks (goethite and hematite) shifted to lower angular values with increasing depth (Fig. 6, inset), thus indicating the lengthening of unit-cell parameters, and thus the probable decrease of Al-for-Fe substitution, since the ionic radius of Al is smaller than Fe (Shannon, 1976). The extent of this substitution was assessed for the two oxides by refinement of the unit-cell parameters and empirical relations between the Al content and the lattice parameters (Schulze, 1984; Stanjek and Schwertmann, 1992). Al substitutions in hematite decreased from 17 mol% (surface) to 10 mol% (deep alteritic horizons) and were almost constant (~ 20 mol%) over the entire profile for goethite. Uncertainty on lattice parameters (and therefore on Al substitution quantification) was low for hematite

owing to the sharp and numerous diffraction peaks, but higher for goethite. Indeed, few isolated diffraction peaks were available for the determination of the unit-cell parameters and peaks were broadened.

The intensity of hematite diffraction lines increased with decreasing depth, thus indicative of a higher proportion of hematite towards the surface, consistent with its status of final alteration product of iron-rich phases (Schwertmann and Latham, 1986). Hematite and goethite are indeed the most thermodynamic stable iron oxides in surface conditions. Amorphous oxides were present as minor constituents since Al and Fe extracted by ascorbate and NH_4OH never exceeded 7% of their HCl/HNO_3 counterparts (Fig. E5). As in pristine soils matrix, KOH extraction likely induced the partial dissolution of gibbsite as $[\text{Al}]_{\text{KOH}}$ was large (median = 51.5% of $[\text{Al}]_{\text{HCl}/\text{HNO}_3}$).

3.3.2 Hg in ferruginous nodules of pristine soils

For surface horizons, $[\text{HgT}]$ were much lower in nodules than in the soil matrix. $[\text{HgT}]$ increased with increasing depth, similar values being obtained for nodules and soil matrix in the deepest sample of acrisol I-1 profile. $[\text{HgT}]$ were even larger in nodules than in soil matrix for ferralsol I-2 samples below 50 cm depth (Fig. E5).

$[\text{HgT}]$ was positively correlated with $[\text{Hg}]_{\text{HCl}/\text{HNO}_3}$ and $[\text{Hg}]_{\text{KOH}}$ ($P < 0.05$) and with $[\text{Fe}]_{\text{HCl}/\text{HNO}_3}$ and $[\text{Al}]_{\text{HCl}/\text{HNO}_3}$ ($P < 0.05$). $(\text{Hg})_{\text{HCl}/\text{HNO}_3}$ extraction yields were larger in ferralsol nodules from deep horizons compared to surface ones. Conversely, in acrisols they were larger for surface horizons. For all nodules these yields scattered about 80%. $(\text{Hg})_{\text{Asco}}$ and $(\text{Hg})_{\text{NH}_4\text{OH}}$ extraction yields rarely exceeded 10% and rapidly decreased with increasing depth in both acrisols and ferralsols. $(\text{Hg})_{\text{KOH}}$ ($44.8 \pm 30.2\%$) extractions yields were systematically larger than the sum $(\text{Hg})_{\text{Asco}} + (\text{Hg})_{\text{NH}_4\text{OH}}$, and progressively decreased downwards in I-1 and I-2 profiles.

3.4 Contaminated gold-mined soils

3.4.1 Granulometry, mineralogy and chemistry

In the gold-mined flat, contaminated gleysols contained a large proportion of gravel size fractions (mainly quartz gravels and stones, mean \pm RSD = $42.7 \pm 24.6\%$ total weight) and the < 2 mm fraction was dominated by sands in contrast with pristine soils (Fig. 2b). Total organic C largely exceeded the concentrations determined in pristine soils and elevated C/N ratios were characteristic of poorly mineralized OM (data not shown). Leaves and wood debris were visible in the litter.

Minerals present in sample SL6 after HCl/HNO₃ extraction were quartz, kaolinite, muscovite, diaspore, rutile and microcline. Gibbsite was for the most part dissolved by HCl/HNO₃, which also possibly partially dissolved kaolinite. The absence of Fe oxides is consistent with the low [Fe]_{HCl/HNO₃} values (0.35 mg.g^{-1}).

Amorphous and crystalline Fe and Al oxides were scarce in contaminated soils as shown by the low Al and Fe concentrations extracted by any reagent compared to pristine soils. For all soil profiles, [Al]_{HCl/HNO₃} and [Fe]_{HCl/HNO₃} were maximum in surface horizons, and sharply decreased to $\sim 5 \text{ mg.g}^{-1}$ at ~ 40 cm depth, except for I1-0, SL0 and G5 profiles.

As for pristine soils, partial gibbsite dissolution by KOH was evidenced by chemistry data as [Al]_{KOH} (median = 76.3% of [Al]_{HCl/HNO₃}) were larger than [Al]_{Asco} (median = 55.7% of [Al]_{HCl/HNO₃}) and [Al]_{NH₄OH} (median = 28.5% of [Al]_{HCl/HNO₃}) (*U* test, $P < 0.05$). Fe oxides were also more attacked by ascorbate ([Fe]_{Asco} median = 31.1% of [Fe]_{HCl/HNO₃}) than by KOH and NH₄OH ([Fe]_{KOH} : median = 17.3% of [Fe]_{HCl/HNO₃} and [Fe]_{NH₄OH} : median = 14.8% of [Fe]_{HCl/HNO₃}).

3.4.2 Hg in contaminated gold mined soils

[HgT] values measured in gleysols from the gold-mined flat (up to $\sim 10 \mu\text{g.g}^{-1}$ in SL6 profile) were up to 5 times higher than those determined in gleysols from the pristine area (Fig. 2b). Although extremely variable, even over very short distances, these values were consistent with those determined in Hg-contaminated soils from different gold-mining regions (Lechler et al., 1997; Lechler et al., 2000; Richard et al., 2000; Sladek and Gustin, 2003), and positively correlated with [Hg] extracted by all four reagents (Tab. 2a and 2b). Contrarily to the pristine area, where gleysols were the pole of lowest [HgT], the only significant correlation of [HgT] with other soil parameters was observed with the sand-size fraction ($P < 0.05$).

μ -XRF map (Fig. 7) shows that Hg was not homogeneously distributed in sample SL6 (30-50cm). Indeed, Hg is essentially present as “hot-spots” of 30 to 100 μm in diameter. In these hot-spots, Hg concentration is not correlated with any element (data not shown), except for a covariation with Au (Fig. 7). These spots are thus likely Hg^0 droplets, possibly amalgamated with Au. Consistently, pyrolysis measurements showed that almost 60% of total Hg was desorbed at 180°C . However, lower percentages of desorbed Hg were determined for SL8 and SL7 samples, thus suggesting that Hg^0 was not systematically the main Hg form over the entire former gold-mined flat (Fig. 8). Consistently, selective extractions have shown that Hg was partially associated to OM and amorphous oxides for some samples as shown by the NH_4OH and ascorbate extraction yields. Such associations remained however minor as $(\text{Hg})_{\text{NH}_4\text{OH}}$ (median = 28.4%) and $(\text{Hg})_{\text{AsCO}}$ (median = 14.7%) extraction yields only seldom exceeded 50 and 30%, respectively (Fig. 8). Relative proportion of Hg associated to refractory minerals was negligible as $(\text{Hg})_{\text{HCl/HNO}_3}$ extraction yields were systematically $\sim 100\%$. In this case, large $(\text{Hg})_{\text{RC}}$ reflect the

proportion related to Hg^0 (Fig.8). KOH extraction yields also were high (median = 86.5%), being always higher than 80% in the uppermost 40 cm.

4. Discussion

4.1 Selective extractions

Further investigation was performed to unravel the reactions leading to Hg reduction and loss during ascorbate extraction, although $[\text{Hg}]_{\text{Asco}}$ were not biased, being calculated from the analysis of the solid residue. Results of the pyrolysis procedure were also questionable as the pyrolysis (180°C) of marine sediment MESS-3 has shown no significant desorption of Hg, while almost 70% of total Hg desorbed from light sandy soil CRM 7002 under the same conditions. It is thus likely that in addition to Hg^0 , Hg bond to OM was partially desorbed during pyrolysis. Pyrolysis temperature (180°C) was indeed close to the temperature range reported by Biester and Scholz (1997) for the thermal release of Hg bound to organic compounds (200-350°C). This is especially relevant for the assessment of the different Hg-compartments in organic-rich contaminated soils.

Cross recoveries between selective extractions were observed for both CRMs and natural samples, but it was also possible to attribute selective mineral extractions to each reagent. The selective character of a given extraction depends on the considered soil matrix, as reagent selectivity depends both on the nature of components present and on their reactivity with respect to a given reagent. Overlapping extractions further increase the uncertainty on the relative proportion of Hg associated to any carrier phase. Although chemical data may help to assess cross recoveries, the restricted and variable selectivity of the different reagents precludes the use of selective extractions as standardized procedures for

environmental studies. Specifically, the use of selective extractions needs preliminary investigation to assess reagent selectivity for a given soil matrix.

4.2 Hg distribution in pristine soils

The study of Hg distribution in a soil has to take into account the original soil cover formation, its current evolution and its present topographic position, that is its position in the soil association (Fritsch et al., 2006). These factors are indeed responsible, at least partially, for the relative abundance and the reactivity of soil organic and mineral components, including Hg carriers, thus providing additional insight in the Hg natural equilibrium and contents.

4.2.1 Hg carrier phases in soil profiles

A positive correlation between the relative amount of the clay-size fraction and C, S, [Fe] and [Al] extracted by HCl/HNO₃, NH₄OH and ascorbate is shown in Table 2. Hg is thus likely associated with finely divided Fe and Al organic complexes and/or with organic coatings on Fe/Al oxides. Several authors have already shown that in Amazonian micro-aggregated horizons, micropeds develop from the bonding between clays, organic matter and iron oxides through the formation of carbon-coatings on mineral surfaces (Tandy et al., 1990; Malengreau and Sposito, 1997; Do Nascimento et al., 2004).

Specific bonding of Hg with sulfur groups from finely divided organic matter may be inferred from the above described correlations for all pristine soils. This is consistent with previous reports of organics, and more especially of reduced sulfur groups, being the most effective sorbents for Hg in acidic environments (pH < ~4.5-5.0), compared to iron oxides and clay minerals (Andersson, 1979; Schuster, 1991; Roulet and Lucotte, 1995; Skyllberg et al., 2000; Skyllberg et al., 2006; Manceau and

Nagy, 2008).

In addition to this essential organic contribution, Hg contents in soils from French Guiana are also controlled by the actual nature of Fe and Al (oxyhydr)oxides (Roulet and Lucotte, 1995; Roulet et al., 1998). In pristine soil matrix, large $[\text{Hg}]_{\text{Asco}}$ and $[\text{Hg}]_{\text{HCl/HNO}_3}$ values were indeed attributed to Al-substituted amorphous and crystalline Fe oxides. As a result of their larger surface areas compared to their crystalline counterparts, amorphous or poorly crystalline species have an increased adsorption capacity, (Schwertmann and Latham, 1986; Schwertmann and Cornell, 2000). The positive correlation between $[\text{Hg}]_{\text{KOH}}$ and $[\text{Al}]_{\text{KOH}}$ supports also the importance of Al oxides as a reservoir for Hg. This reservoir is accessible through KOH and, to a lesser extent, through ascorbate extractions, thus the large $[\text{Al}]_{\text{Asco}}$ plead for the partial dissolution of (amorphous) Al (oxyhydr)oxides (Schwertmann and Latham, 1986).

In nodules, as in soil matrix, Hg is bond to Al and Fe oxides. Ferruginous nodules are abundant in ferralsols and acrisols, where they represent ~50% of total soil materials and thus represent large Hg reservoirs, $[\text{HgT}]$ being similar in nodules and soil matrix. In addition to Al-substituted hematite and goethite, gibbsite contributes significantly to Hg retention in soil nodules, especially in surface horizons, as suggested by the large $(\text{Hg})_{\text{KOH}}$ extraction yields associated with large $[\text{Al}]_{\text{KOH}}$ values. This observation is consistent with the strong affinity of Hg(II) for gibbsite (Kim et al., 2004a; Kim et al., 2004b; Weerasooriya et al., 2007).

Finally, the contribution of refractory minerals (identified as muscovite, anatase, rutile and kaolinite) is non negligible, although minor, in pristine soils as the median $(\text{Hg})_{\text{HCl/HNO}_3}$ extraction yield is only 89.8%.

4.2.2 Influence of soil structure on Hg distribution in soil profiles

From the above description, it appears that the vertical distribution of OM, Al/Fe (oxyhydr)oxides and ferruginous nodules in the soil matrix rules Hg distribution. In the following section, pedological and chemical characteristics responsible for the spatial distribution of these components in soil profiles will be discussed.

Upslope, large [HgT] have been measured in the matrix of the ferralsol micro-aggregated horizons (i.e., A and B horizons). The micro-aggregated structure confers a good water drainage capacity to ferralsols, favoring water flow and oxidizing conditions. As a result, Hg is spread throughout these micro-aggregated horizons as the result of both significant leaching and migration of atmospheric inputs (Guedron et al., 2006). Plant litter is rapidly mineralized in surface horizons, and the rapid turnover of humic substances leads to the migration of fulvic acids in deeper organo-mineral horizons where they are complexed to Fe and Al oxides (Roulet and Lucotte, 1995). Thus, Hg originating from plant litter decomposition and/or from atmospheric fallouts can migrate into the organo-mineral horizons as organic-Hg complexes and progressively adsorb onto Al/Fe (oxyhydr)oxides. Soil ecosystem engineers (soil invertebrates and roots) also play an important role in the particulate transfer of Hg by enhancing aggregation (Velasquez et al., 2007) and soil hydraulic conductivity (Grimaldi et al., 2008) through biogenic soil organization. In the micro-aggregated B horizon of ferralsols, the distribution of amorphous Fe oxides is positively correlated to [HgT], although their relative abundance is lower than or similar to that of the crystalline varieties. The comparison of $[\text{Fe}]_{\text{Cryst}}$ and $[\text{Fe}]_{\text{Asco}}$ indicates that the relative proportion of crystalline Fe oxides is increased further in the superficial layer and in the deep alteritic horizons compared to the micro-aggregated B horizon of ferralsols. In addition, the positive correlations between $[\text{Hg}]_{\text{RC}}$ and $[\text{Fe}]_{\text{Cryst}}$ or $[\text{Al}]_{\text{Cryst}}$

throughout the entire soil profile suggest that $[Hg]_{RC}$ is partially associated to Al-substituted crystalline Fe oxides. In this case, the sum of $[Hg]$ adsorbed onto amorphous and crystalline Fe oxides would be comparable or larger than the part related to organic compounds.

The micro-aggregated structure of ferralsols disappears progressively with increasing depth, giving rise to deep mineral horizons with a continuous structure composed of large mineral relics. Parental material relics “dilute” Al/Fe oxides and thus reduce the overall sorption capacity of deep horizons. Another essential factor is the lower permeability of deep horizons which limits the downward migration of Hg (Guedron et al., 2006). Hg content thus mainly results from rock weathering and pedogenesis (Guedron et al., 2006), $[HgT]$ being mainly associated with coarse-grained goethite and hematite.

In ferralsol nodules, Hg is mainly bond to Al-substituted hematite and goethite, and to gibbsite. As in ferralsol matrix, highest $[HgT]$ values were measured in the micro-aggregated horizon. Indeed, the downward decrease of $(Hg)_{HCl/HNO_3}$ extraction yields and the mineralogical evolution suggest that A and B horizons nodules are primarily composed of neo-formed minerals, thus indicating an advanced stage of pedogenesis and weathering in superficial horizons. Mineral neoformation also appears to favor the incorporation of atmospheric Hg inputs.

Halfway down the slope, in acrisols, a similar mineralogical and structural contrast is observed between superficial (A and B horizons) and alteritic horizons. This transition is sharp as evidenced by the increase of the silt fraction and by the decrease of $[HgT]$. As for ferralsol, the increase of refractory minerals with increasing depth is most likely responsible for the observed decrease of $[HgT]$.

Downslope, in gleysols, [HgT] were lower since fine organic fraction, S and amorphous oxides are less abundant than upslope, even though carrier phases were similar to those identified in ferralsols and Acrisols. Gleysols are depleted in iron oxides and the main minerals are kaolinite, gibbsite, muscovite and quartz. Hg extracted by NH_4OH never exceeds 40% of [HgT] in gleysol surface horizons and rapidly decreases with depth. Hg bound to amorphous oxides never exceeds 20% of [HgT], and almost 50% of [HgT] is likely associated to Al-substituted crystalline Fe oxides, gibbsite and to refractory minerals. Consistently, Hg, Fe, and Al extracted by HCl/HNO_3 are together positively correlated in the gleysol profile. In depth, Hg is less abundant and mainly associated to refractory minerals since $(\text{Hg})_{\text{RC}}$ extraction yields increase with increasing depth.

4.2.3 Influence of soil formation on the distribution of Hg over the soil association

The soil association results from the ferralsols current imbalance, which leads to temporal and spatial evolutions (Boulet et al., 1993; Grimaldi et al., 2004). Because of their major role as Hg reservoirs, the following description of Hg distribution along the toposequence will thus focus on OM and Fe oxides behavior in the soil association.

In organic horizons, the [HgT] decrease along the slopes correlates with the decrease of their C and S contents. However, organic horizons in gleysols are characterized by an increased proportion of OM in gravel size fractions ($> 2 \text{ mm}$) and thus by a lower degree of mineralization of coarse OM because of hydromorphy. Consequently, the overall reactivity of coarse OM towards Hg (including the reactivity of S groups) decreases when all soil fractions are considered even if C and S remain abundant (Andersson, 1979; Kerndorff and Schnitzer, 1980; Schnitzer and Kerndorff, 1981; Ochs et al., 1994; Gasper et al., 2007).

The decreasing proportion of Fe and Al (oxyhydr)oxides down the slope results from the combined effect of diffuse erosion and leaching due to the lateral drainage of horizons overlying the alteritic horizons of Acrisols and of the progressive occurrence of hydromorphy (Boulet et al., 1979; Fritsch et al., 1986; Fritsch et al., 2006; Grimaldi et al., 2004; Lucas et al., 1996). Drainage induces a texture coarsening from the original clayey texture of Ferralsols to the sandy-loam texture of Gleysols, whereas hydromorphy induces the dissolution of crystalline and amorphous Al-bearing Fe oxides and the export of the reduction products through the hydrographic network (Grimaldi et al., 2008). Both processes result in the relative increase of coarse fractions composed mainly of quartz and neoformed kaolinite (Boulet, 1978; Roulet et al., 1998) which possess a low affinity for Hg (Sarkar et al., 1999; Sarkar et al., 2000).

4.3 Influence of former gold mining activities on anthropogenic Hg pool in soils

In contrast to pristine soils, Hg appears to be associated mainly with the prevailing sandy fraction. In highly contaminated sites Hg has been identified as Hg⁰, insoluble cinnabar and metacinnabar (Lechler et al., 1997; Slowey et al., 2005; Slowey and Brown, 2007). In the present study, mercury sulfides (cinnabar and metacinnabar) are most likely insignificant as no positive correlation was found between Hg and S. (Hg)_{HCl/HNO₃} extraction yields are systematically close to 100% and support further the low amount of mercury sulfides which are essentially insoluble in concentrated HCl/HNO₃ (Mikac et al., 2002; Mikac et al., 2003).

The probable presence of Hg⁰ is supported by the observation of macroscopic Hg⁰ droplets during a prospective “panning” in the sandy horizon of gold-mined Gleysols (50-100 cm depth) next to profile III-0. It was however impossible to assess

the distribution of the Hg^0 droplets along vertical profiles. μXRF confirmed the presence of isolated Hg^0 droplets ($\sim 100\text{ }\mu\text{m}$ in diameter) in sample SL6 (30-50cm), possibly amalgamated with micrometric gold particles. Consistently, pyrolysis measurements have shown that Hg^0 generally prevail in the former gold-mined flat soils, with some exceptions (e.g., SL7 and SL8 profiles). In the latter profiles, the reduced contribution of Hg^0 can result from its oxidation, known to be fast in tropical environments (Dominique et al., 2007). If geochemical conditions are not permanently reducing, as in the surface horizons, Hg^0 can be oxidized, allowing adsorption onto OM and minerals. The relative proportion of Hg bond to OM is however lower than in pristine soils, $(\text{Hg})_{\text{NH}_4\text{OH}}$ extraction yields rarely exceeding 50%. As previously discussed, the overall limited mineralization of OM is most likely responsible for the low reactivity of OM for Hg. Similarly, the relative proportion of Hg bond to amorphous Fe oxides is low (up to 15%), these oxides being scarce in hydromorphic environments. Finally, the part related to refractory minerals (i.e., quartz, kaolinite and muscovite) appears to be negligible since $(\text{Hg})_{\text{HCl/HNO}_3}$ extraction yields are always close to 100%.

5. Conclusion

The combination of selective extractions with physical techniques (XRD and μXRF) significantly improved the determination of Hg speciation by allowing the identification of Hg carrier phases targeted by the different extractants. However, the quantification of Hg associated to a given carrier phase is affected by intrinsic bias, especially because of probable overlaps between the different extraction procedures. Thus, selective extractions can not be used as a standard procedure for natural

691 samples since the use of selective extractions requires the preliminary assessment of
692 reagent selectivity for a given soil matrix.

693 By coupling XRD and selective extractions, the main Hg carrier phases in
694 pristine soils were identified as sulfur groups from organic matter, amorphous and
695 crystalline Al-substituted Fe oxides and, to a lower extent, Al oxides. The relative
696 contribution of these carriers to the overall Hg concentration was dependent on their
697 relative abundance which is controlled by the pedogenetic evolution along the slopes,
698 and more especially by redox conditions, hydric properties, and ecosystem
699 engineers. In the former gold-mined flat, Hg was found mainly as Hg^0 , possibly
700 amalgamated with Au, and as oxidized Hg^{II} associated with organic matter, Fe and/or
701 Al oxides in surface horizons.

702 *5.1 Concluding Remarks*

703 These findings have major implications on the contamination of hydrosystems
704 in tropical regions, where soil erosion due to deforestation, gold mining and
705 agricultural processes are intense and lead to the release of Hg-rich clay-size
706 particles as shown by the low proportion of clay-size fractions in gold-mined gleysols.
707 When entering suboxic and anoxic environments (e.g. river or dam sediments), Hg
708 bond to clay-size particles indeed becomes accessible to ferri- and sulfato-reducing
709 bacteria that are the main factors of Hg methylation (Fitzgerald and Lamborg, 2003;
710 Fleming et al., 2006). Hg bound to OM and Fe oxides is specifically concerned as
711 these major components of the clay-size fraction are essential nutrients for
712 methylating micro-organisms and final electron acceptors of their metabolism. In
713 addition, former gold mined soils are potential important sources of Hg for
714 methylating bacteria. Indeed, Dominique et al. (2007) have shown that anthropogenic

Hg⁰ from former gold-mining activities also promotes the production of MMHg in the Amazonian hydrosystems and its availability to trophic webs.

Acknowledgments

This research was supported mainly by the CNRS through its “Mercury in French Guiana” research program and by the Boulanger Mine Company (CMB – Cayenne) through a Ph.D. granted to Stéphane Guédron. The authors thank Manuel Munoz and Mathieu Corazzi (LGCA – Grenoble) for the assistance with μ XRF mapping, Vincent Perrot and Nicolas Geoffroy (LGIT – Grenoble) for technical support during the project, and Max Sarrazin (IRD – Cayenne) who performed soil granulometry and C, N and S analyses.

References

- Andersson, A., 1979. Mercury in soils. In: J.O. Nriagu (Editor), The biogeochemistry of mercury in the environment. Elsevier, Amsterdam, pp. 80-111.
- Avery, B.W. and Bascomb, C.L., 1974. Soil survey laboratory methods. Technical Monograph, 6. Soil Survey of England and Wales, Harpenden.
- Barbosa, A.C., Souza, J.D., Dorea, J.G., Jardim, W.F. and Fadini, P.S., 2003. Mercury Biomagnification in a Tropical Black Water, Rio Negro, Brazil. Arch. Environ. Contam. Toxicol. 45(2): 235-246.
- Barret, J., 2004. Illustrated Atlas of French Guyana. French Guyana Publications, Cayenne, 219 pp (in French).
- Battke, F., Ernst, D., Fleischmann, F. and Halbach, S., 2008. Phytoreduction and volatilization of mercury by ascorbate in Arabidopsis thaliana, European beech and Norway spruce. Appl. Geochem. 23(3): 494-502.

738 Beldowski, J. and Pempkowiak, J., 2003. Horizontal and vertical variabilities of
 739 mercury concentration and speciation in sediments of the Gdansk Basin,
 740 Southern Baltic Sea. *Chemosphere*. 52: 645-654.

741 Beldowski, J. and Pempkowiak, J., 2007. Mercury transformations in marine coastal
 742 sediments as derived from mercury concentration and speciation changes
 743 along source/sink transport pathway (Southern Baltic). *Estuarine Coastal Shelf*
 744 *Sci.* 72(1-2): 370-378.

745 Benoit, J.M., Gilmour, C.C., Heyes, A., Mason, R.P. and Miller, C.L., 2003.
 746 Geochemical and biological controls over methylmercury production and
 747 degradation in aquatic ecosystems. In: Y. Cai and O.C. Braids (Editors),
 748 *Biogeochemistry of Environmentally Important Trace Elements*. Oxford
 749 University Press, pp. 262-297.

750 Biester, H., 1994. Möglichkeiten der anwendung eines temperaturgesteuerten
 751 pyrolyseverfahrens zur bestimmung der bindungsform des quecksilbers in
 752 boden und sedimenten. *Heidelberger Geowiss. Abh.* 75, 156 pp.

753 Biester, H. and Scholz, C., 1997. Determination of mercury binding forms in
 754 contaminated soils: Mercury pyrolysis versus sequential extractions. *Environ.*
 755 *Sci. Technol.* 31: 233-239 (in German).

756 Bloom, N.S. and Fitzgerald, W.F., 1988. Determination of volatil mercury species at
 757 the picogram level by low-temperature gas chromatography with cold-vapor
 758 atomic fluorescence detection. *Anal. Chim. Acta.* 208: 151-161.

759 Bloom, N.S., Preus, E., Katon, J. and Hiltner, M., 2003. Selective extractions to
 760 assess the biogeochemically relevant fractionation of inorganic mercury in
 761 sediments and soils. *Anal. Chim. Acta.* 479: 233-248.

- Bollen, A., Wenke, A. and Biester, H., 2008. Mercury speciation analyses in HgCl₂-contaminated soils and groundwater - Implications for risk assessment and remediation strategies. *Water Res.* 42(1-2): 91-100.
- Boszke, L., Kowalski, A., Szczuciński, W., Rachlewicz, G., Lorenc, S.A. and Siepak, J., 2006. Assessment of mercury mobility and bioavailability by fractionation method in sediments from coastal zone inundated by the 26 December 2004 tsunami in Thailand. *Environ. Geol.* 51(4): 527-536.
- Boulet, R., 1978. Existence of high lateral differentiation systems in French Guiana's ferrallitic soils: a new example of an imbalanced pedological cover. *Soil Sci.* 2: 75-82 (in French).
- Boulet, R., Grugiere, J.M. and Humbel, F.X., 1979. Relationships between soil organization and water dynamics of septentrional French Guiana. Agronomic consequences of an evolution controlled by a mainly tectonic disequilibrium. *Soil Sci.* 1: 3-18 (in French).
- Boulet, R., Lucas, Y., Fritsch, E. and Paquet, H., 1993. Landscape geochemistry: role of soil cover. In: French. Acad. Sci. (Editor), *Sedimentology and surface geochemistry*, Paris, pp. 55-76 (in French).
- Brabo, E.S., Angelica, R.S., Silva, A.P., Faial, K.R.F., Mascarenhas, A.F.S., Santos, E.C.O., Jesus, I.M. and Loureiro, E.C.B., 2003. Assessment of mercury levels in soils, waters, bottom sediments and fishes of the Acre state in Brazilian Amazon. *Water Air Soil poll.* 147: 61-77.
- Bravard, S. and Righi, D., 1991. Characterization of fulvic and humic acids from an oxisol-spodosol toposequence of Amazonia, Brazil. *Geoderma.* 48(1-2): 151-162.

786 Carmouze, J.P., Lucotte, M. and Boudou, A., 2001. Le Mercure en Amazonie Rôle
787 de l'homme et de l'environnement, Risques sanitaires. IRD Editions, Bondy,
788 494 pp (in French).

789 Charlet, L. and Sposito, G., 1987. Monovalent ion adsorption by an oxisol. Soil Sci.
790 Soc. Am. J. 51: 1155-1160.

791 Charlet, L. and Sposito, G., 1989. Bivalent ion adsorption by an Oxisol. Soil Sci. Soc.
792 Am. J. 53(5): 691-695.

793 Coquery, M., Cossa, D. and Sanjuan, J., 1997. Speciation and sorption of mercury in
794 two macro-tidal estuaries. Marine Chem. 58(1-2): 213-227.

795 Coquery, M., Cossa, D., Azemard, S., Peretyazhko, T. and Charlet, L., 2003.
796 Methylmercury formation in the anoxic waters of the Petit-Saut reservoir
797 (French Guiana) and its spreading in the adjacent Sinnamary river. J. Phys.
798 IV. 107: 327-331.

799 Cossa, D. and Gobeil, C., 2000. Mercury speciation in the Lower St. Lawrence
800 estuary. Can. J. Fish. Aquat. Sci. 57: 138-147.

801 De Oliveira, S.M.B., Melfi, A.J., Fostier, A.H., Forti, M.C., Favaro, D.I.T. and Boulet,
802 R., 2001. Soils as an important sink for mercury in the Amazon. Water Air Soil
803 Poll. 26: 321-337.

804 Deckers, J., Nachtergaele, F. and Spaargaren, O., 1998. World reference base for
805 soil resources. ACCO Publishers, 165 pp.

806 Di Giulio, R.T. and Ryan, E.A., 1987. Mercury in soils, and clams from a North
807 Carolina peatland. Water, Air and soil poll. 33: 205–219.

808 Do Nascimento, N.R., Bueno, G.T., Fritsch, E., Herbillon, A.J., Allard, T., Melfi, A.J.,
809 Astolfo, R., Boucher, H. and Li, Y., 2004. Podzolization as a deferralitization

process: a study of an Acrisol-Podzol sequence derived from Palaeozoic sandstones in the northern upper Amazon Basin. *Eur. J. Soil Sci.* 55: 523-538.

Do Valle, C.M., Santana, G.P., Augusti, R., Egreja Filho, F.B. and Windmoller, C.C., 2005. Speciation and quantification of mercury in Oxisol, Ultisol, and Spodosol from Amazon (Manaus, Brazil). *Chemosphere*. 58(6): 779-792.

Doering, E.R., Havrilla, G.J. and Miller, T.C., 2004. Disilicide Diffusion Coating Inspection by Micro X-Ray Fluorescence Imaging. *J. Nondestr. Eval.*, 23(3): 95-105.

Dominique, Y., Muresan, B., Duran, R., Richard, S. and Boudou, A., 2007. Simulation of the Chemical Fate and Bioavailability of Liquid Elemental Mercury Drops from Gold Mining in Amazonian Freshwater Systems. *Environ. Sci. Tech.* 41(21): 7322 -7329.

Eagenhouse, R.P., Young, D.R. and Johnson, J.N., 1978. Geochemistry of mercury in Palos Verdes sediments. *Environ. Sci. Technol.* 12: 1151–1157.

Evain, M., 1992. U-FIT: A Cell Parameter Refinement Program. IMN Nantes.

Fitzgerald, W.F. and Lamborg, C.H., 2003. Geochemistry of mercury in the environment. In: B. Sherwood Lollar (Editor), *Treatise on Geochemistry*. Elsevier, pp. 107-148.

Fleming, E.J., Mack, E.E., Green, P.G. and Douglas, C.N., 2006. Mercury methylation from unexpected sources: molybdate-inhibited freshwater sediments and iron-reducing bacterium. *Appl. Environ. Microbiol.* 72(1): 457-464.

Fontes, M.P.F. and Gomes, P.C., 2003. Simultaneous competitive adsorption of heavy metals by the mineral matrix of tropical soils. *Appl. Geochem.* 18(6): 795-804.

835 Frery, N., Maury-Brachet, R., Maillot, E., Deheeger, M., Merona de, B. and Boudou,
836 A., 2001. Goldmining activities and mercury contamination of native
837 Amerindian communities in french Guiana: key role of fish in dietary uptake.
838 Environ. Health Persp. 109: 449-456.

839 Fritsch, E., Bocquier, G., Boulet, R., Dosso, M. and Humbel, F.X., 1986.
840 Transforming systems of ferrallitic cover in French Guiana, structural analysis
841 of a supergene formation and mode of representation. ORSTOM notebook,
842 Pedol. Ser. 12(4): 361-395 (in French).

843 Fritsch, E., Morin, G., Bedidi, A., Bonnin, D., Balan, E., Caquineau, S. and Calas, G.,
844 2005. Transformation of haematite and Al-poor goethite to Al-rich goethite and
845 associated yellowing in a ferrallitic clay soil profile of the middle Amazon Basin
846 (Manaus, Brazil). Eur. J. Soil Sci. 56(5): 575-588.

847 Fritsch, E., Herbillon, A.J., doNascimento, N.R., Grimaldi, M. and Melfi, A.J., 2006.
848 From Plinthic Acrisols to Plinthosols and Gleysols: iron and groundwater
849 dynamics in the tertiary sediments of the upper Amazon basin. Eur. J. Soil Sci.
850 58: 989-1006.

851 Gasper, J.D., Aiken, G.R. and Ryan, J.N., 2007. A critical review of three methods
852 used for the measurement of mercury (Hg^{2+})-dissolved organic matter stability
853 constants. Appl. Geochem. 22(8): 1583-1597.

854 Grimaldi, C., Grimaldi, M., Millet, A., Bariac, T. and Boulègue, J., 2004. Behavior of
855 chemical solutes during a storm in a rainforested headwater catchment.
856 Hydrol. Process. 18: 93-106.

857 Grimaldi, C., Guedron, S. and Grimaldi, M., 2008. Mercury distribution in tropical soil
858 profiles related to origin of mercury and soil processes. Sci. Total Environ.
859 401: 121-129.

860 Grimaldi, M., Gaudet, J.P., Grimaldi, C., Melieres, M.A. and Spadini, L., 2001.
861 Sources, budget and transfers in soils and sediments. In: CNRS (Editor),
862 Mercury in French Guiana research Program. Final report, part one: the region
863 of Saint Elie and the Petit Saut reservoir. CNRS-PEVS, pp. 5-15 (in French).

864 Guedron, S., Grimaldi, C., Chauvel, C., Spadini, C. and Grimaldi, M., 2006.
865 Weathering versus atmospheric contributions to mercury concentrations in
866 French Guiana soils. *Appl. Geochem.* 21: 2010-2022.

867 Guehl, J.M., 1984. Water dynamic in French Guiana tropical humid forest soil.
868 Influence of the pedological cover . *Ann. For. Sci.* 41(2): 195–236 (in French).

869 Kerndorff, H. and Schnitzer, M., 1980. Sorption of metals on humic acid . *Geochim.*
870 *Cosmochim. Acta.* 44: 1701-1708.

871 Khwaja, A., Bloom, P.R. and Brezonik, P.L., 2006. Binding constants of divalent
872 Mercury (Hg^{2+}) in soil humic acids and soil organic matter. *Environ. Sci.*
873 *Technol.* 40: 844-849.

874 Kim, C., Rytuba, J. and Brown, J.G.E., 2004a. EXAFS study of mercury (II) sorption
875 to Fe- and Al- (hydr)oxides I. Effect of chloride and sulfate. *J. Colloid Interface*
876 *Sci.* 270: 9-20.

877 Kim, C., Rytuba, J.J. and Brown, J.G.E., 2004b. EXAFS study of mercury (II) sorption
878 to Fe- and Al- (hydr)oxides I. Effect of pH. *J. Colloid Interface Sci.* 271: 1-15.

879 Kostka, J.E. and Luther III, G.W., 1994. Partitioning and speciation of solid phase
880 iron in saltmarsh sediments. *Geochim. Cosmochim. Acta.* 58(7): 1701–1710.

881 Lacerda, L.D., 1997. Global mercury emissions from gold and silver mining. *Water*
882 *Air Soil Poll.* 97: 209-221.

883 Lebel, J., Mergler, D., Lucotte, M., Amarin, M., Dolbec, J., Miranda, D., Arantes, G.,
884 Rhéault, I. and Pichet, P., 1996. Evidence of early nervous system dysfunction

885 in Amazonian populations exposed to low levels of methylmercury.
886 Neurotoxicol. 17: 157-168.

887 Lechler, P.J., Miller, J.R., Hsu, L.-C. and Desilets, M.O., 1997. Mercury mobility at the
888 Carson River Superfund Site, west-central Nevada, USA: Interpretation of
889 mercury speciation data in mill tailings, soils, and sediments. J. Geochem.
890 Explor. 58(2-3): 259-267.

891 Lechler, P.J., Miller, J.R., Lacerda, L.D., Vinson, D., Bonzongo, J.-C., Lyons, W.B.
892 and Warwick, J.J., 2000. Elevated mercury concentrations in soils, sediments,
893 water, and fish of the Madeira River basin, Brazilian Amazon: a function of
894 natural enrichments? Sci. Total Environ. 260: 87-96.

895 Leermakers, M., Baeyens, W., Quevauviller, P. and Horvat, M., 2005. Mercury in
896 environmental samples: Speciation, artifacts and validation. Trends Anal.
897 Chem. 24(5): 383-393.

898 Lucas, Y., Nahon, D., Cornu, S. and Eyrolle, F., 1996. Soil genesis and dynamics in
899 equatorial areas. C. R. Acad. Sci. 322(1): 1-16 (In French).

900 Malengreau, N. and Sposito, G., 1997. Short-time dissolution mechanisms of
901 kaolinitic tropical soils. Geochim. Cosmochim. Acta; 61(20): 4297-4307.

902 Manceau, A. and Nagy, K.L., 2008. Relationships between Hg(II)–S bond distance
903 and Hg(II) coordination in thiolates. Dalton Trans. 11: 1385–1508.

904 Mikac, N., Foucher, D., Niessen, S. and Fischer, J.-C., 2002. Extractability of HgS
905 (cinnabar and metacinnabar) by hydrochloric acid. Anal. Bioanal. Chem.
906 374(6): 1028-1033.

907 Mikac, N., Foucher, D., Niessen, S., Lojen, S. and Fischer, J.-C., 2003. Influence of
908 chloride and sediment matrix on the extractability of HgS (cinnabar and
909 metacinnabar) by nitric acid. Anal. Bioanal. Chem. 377(7): 1196-1201.

910 Milési, J.P., Egal, E., Ledru, P., Vernhet, Y., Thiéblemont, D., Cocherie, A., Tegye, Y.,
 911 M., Martel-Jantin, B. and Lagny, P., 1995. Mineralizations of the northern
 912 French Guiana in their geological setting. *Mining Res. Chron.* 518: 5-58 (in
 913 French).
 914 Molicova, H., Grimaldi, M., Bonell, M. and Hubert, P., 1997. Using TOPMODEL
 915 towards identifying and modelling the hydrological patterns within a headwater
 916 humid, tropical catchment. *Hydrolog. Process.* 11: 1169-1196.
 917 Ochs, M., Cosovic, B. and Stumm, W., 1994. Coordinative and hydrophobic
 918 interaction of humic substances with hydrophilic Al_2O_3 and hydrophobic
 919 mercury surfaces. *Geochim. Cosmochim. Acta.* 58(2): 639-650.
 920 Richard, S., Arnoux, A., Cerdan, P., Reynouard, C. and Horeau, V., 2000. Mercury
 921 levels of soils, sediments and fish in French Guiana, South America. *Water Air
 922 Soil Poll.* 124: 221-244.
 923 Rodriguez Martin-Doimeadios, R.C., Wasserman, J.C., Garcia Bermejo, L.F.,
 924 Amouroux, D., Berzas Nevado, J.J. and Donard, O.F.X., 2000. Chemical
 925 availability of mercury in stream sediments from the Almaden area, Spain. *J.
 926 Environ. Monit.* 2: 360-366.
 927 Roos-Barraclough, F., Givélet, N., Martinez-Cortizas, A., Goodsite, M.E., Biester, H.
 928 and Shotyk, W., 2002. An analytical protocol for determination of total mercury
 929 concentration in solid peat samples. *Sci. Tot. Environ.* 292: 129-139.
 930 Roulet, M. and Lucotte, M., 1995. Geochemistry of mercury in pristine and flooded
 931 ferrallitic soil of a tropical rain forest in French Guiana, South America. *Water,
 932 Air, Soil Poll.* 80: 1079-1088.
 933 Roulet, M., Lucotte, M., Saint-Aubin, A., Tran, S., Rheault, I., Farella, N., Da Silva,
 934 E.D., Dezencourt, J., Passos, C.J.S., Soares, G.S., Guimaraes, J.R.D.,

935 Mergler, D. and Amorim, M., 1998. The geochemistry of mercury in central
 936 Amazonian soils developed on the Alter-do-Chao formation of the lower
 937 Tapajos River Valley, Para state, Brazil. *Sci. Total Environ.* 223(1): 1-24.

938 Rowell, D.L., 1994. *Soil Science : methods and applications*. British Library, Harlow
 939 (England).

940 Sanchez, D.M., Quejido, A.J., Fernandez, M., Hernandez, C., Schmid, T., Millan, R.,
 941 Gonzalez, M., Aldea, M., Martan, R. and Morante, R., 2005. Mercury and trace
 942 element fractionation in Almaden soils by application of different sequential
 943 extraction procedures. *Anal. Bioanal. Chem.* 381(8): 1507-1513.

944 Sarkar, D., Essington, M.E. and Misra, K.C., 1999. Adsorption of mercury(II) by
 945 variable charge surfaces of quartz and gibbsite. *Soil Sci. Soc. Am. J.* 63:
 946 1626-1636.

947 Sarkar, D., Essington, M.E. and Misra, K.C., 2000. Adsorption of mercury(II) by
 948 kaolinite. *Soil Sci. Soc. Am. J.* 64: 1698-1975.

949 Schnitzer, M. and Kerndorff, H., 1981. Reactions of fulvic acid with metal ions. *Water,*
 950 *Air, Soil Poll.* 15: 97-108.

951 Schulze, D.G., 1984. The influence of aluminium on iron oxides. VIII. Unit-cell
 952 dimension of Al-substituted goethites and estimation of Al from them. *Clays*
 953 *Clay Miner.* 32(1): 36-44.

954 Schuster, E., 1991. The behavior of mercury in the soil with special emphasis on
 955 complexation and adsorption processes- a review of the literature. *Water Air*
 956 *Soil Poll.* 56: 667-680.

957 Schwertmann, U. and Latham, M., 1986. Properties of iron oxides in some new
 958 caledonian oxisols. *Geoderma.* 39: 105-123.

959 Schwertmann, U. and Cornell, R.M., 2000. Iron oxides in the laboratory : preparation
 960 and characterization. Wiley-VCH, Weinheim, 188 pp.

961 Shannon, R., 1976. Revised effective ionic radii and systematic studies of interatomic
 962 distances in halides and chalcogenides. *Acta Crystallogr.* 32(5): 751-767.

963 Skyllberg, U., Xia, K., Bloom, P.R., Nater, E.A. and Bleam, W.F., 2000. Binding of
 964 mercury(II) to reduced sulfur in soil organic matter along upland-peat soil
 965 transects. *J. Environ. Qual.* 29: 855-865.

966 Skyllberg, U., Bloom, P.R., Qian, J., Lin, C.-M. and Bleam, W.F., 2006. Complexation
 967 of Mercury(II) in Soil Organic Matter: EXAFS Evidence for Linear Two-
 968 Coordination with Reduced Sulfur Groups. *Environ. Sci. Technol.* 40(13):
 969 4174-4180.

970 Sladek, C. and Gustin, M.S., 2003. Evaluation of sequential and selective extraction
 971 methods for determination of mercury speciation and mobility in mine waste.
 972 *Appl. Geochem.* 18(4): 567-576.

973 Slowey, A.J., Rytuba, J.J. and Brown, J.G.E., 2005. Speciation of mercury and mode
 974 of transport from placer Gold Mine Tailings. *Environ. Sci. Technol.* 39(6):
 975 1547-1554.

976 Slowey, A.J. and Brown, J.G.E., 2007. Transformations of mercury, iron, and sulfur
 977 during the reductive dissolution of iron oxyhydroxide by sulfide. *Geochim.*
 978 *Cosmochim. Acta.* 71(4): 877-894.

979 Stanjek, H. and Schwertmann, U., 1992. The influence of aluminium on iron oxides.
 980 Part XVI: hydroxyl and aluminium substitution on synthetic hematites. *Clays*
 981 *Clay Miner.* 40(3): 347-354.

982 Tandy, J.C., Grimaldi, M., Grimaldi, C. and Tessier, D., 1990. Mineralogical and
 983 textural changes in French Guiana oxisols and their relation with

984 microaggregation. In: L.A. Douglas (Editor), Soil micromorphology. A basic
 985 and applied science. 8. International Working Meeting of Soil
 986 Micromorphology. Developments in Soil Science. Elsevier, Amsterdam, pp.
 987 191-198.

988 Trivedi, P. and Axe, L., 2001. Ni and Zn Sorption to Amorphous versus Crystalline
 989 Iron Oxides: Macroscopic Studies. J. Colloid Interface Sci., 244: 221-229.

990 Veiga, M. and Baker, R., 2004. Protocols for environmental and health assessment
 991 of mercury released by artisanal and small scale miners. Report to the Global
 992 mercury project: removal of barriers to introduction of cleaner artisanal gold
 993 mining and extraction technologies, GEF/UNDP/UNIDO; 2004. p. 170.

994 Velasquez, E., Pelosi, C., Brunet, D., Grimaldi, M., Martins, M., Rendeiro, A.C.,
 995 Barrios, E. and Lavelle, P., 2007. This ped is my ped: Visual separation and
 996 near infrared spectra allow determination of the origins of soil
 997 macroaggregates. Pedobiologia. 51(1): 75-87.

998 Wallschlager, D., Desai, M.V.M., Spengler, M. and Wilken, R.-D., 1998. Mercury
 999 speciation in floodplain soils and sediments along a contaminated river
 1000 transect. J. Environ. Qual. 27: 1034-1044.

1001 Webster, R., 2001. Statistics to support soil research and their presentation. Eur. J.
 1002 Soil Sci. 52(2): 331-340.

1003 Weerasooriya, R., Tobschall, H.J., Seneviratne, W. and Bandara, A., 2007.
 1004 Transition state kinetics of Hg(II) adsorption at gibbsite-water interface. J.
 1005 Hazard. Mater. 147(3): 971-978.

1006 Wentworth, C.K., 1922. A scale of grade and class terms for clastic sediments. J.
 1007 Geol. 30: 377-392.

1008

Table 1: Pearson correlation matrix (correlation coefficient (CC), P value (P) and number of samples (N)) of pristine soils extracted Hg, Hg extraction yields, Fe, Al, Clay size fraction, Fine silts, C and S for total and (a) HCl/HNO₃ (labeled HCl) and ascorbate (labeled Asco) selective extractions, and (b) KOH and NH₄OH selective extractions.

Table 1a

	Stati	[Hg] _{HCl} (µg g ⁻¹)	(Hg) _{HCl} (%)	[Fe] _{HCl} (mg g ⁻¹)	[Al] _{HCl} (mg g ⁻¹)	Clay (g/100g)	Silt (g/100g)	C (g/100g)	S (g/100g)		[Hg] _{KOH} (µg g ⁻¹)	(Hg) _{KOH} (%)	[Fe] _{KOH} (mg g ⁻¹)	[Al] _{KOH} (mg g ⁻¹)	Clay (g/100g)	Silt (g/100g)	C (g/100g)	S (g/100g)
[HgT] (µg g⁻¹)	CC	1.00	0.45	0.19	0.15	0.59	- 0.60	0.42	0.62	[HgT] (µg g⁻¹)	0.89	0.32	0.33	0.37	0.59	- 0.60	0.42	0.62
	P	1.E-41	3.E-03	2.E-01	3.E-01	9.E-05	7.E-05	7.E-03	2.E-05		7.E-14	5.E-02	5.E-02	3.E-02	9.E-05	7.E-05	7.E-03	2.E-05
	N	40	40	40	40	38	38	40	40		38	38	36	36	38	38	40	40
[Hg]_{HCl} (µg g⁻¹)	CC		0.48	0.18	0.13	0.56	- 0.57	0.40	0.58	[Hg]_{KOH} (µg g⁻¹)		0.63	0.21	0.15	0.48	- 0.42	0.26	0.51
	P		2.E-03	3.E-01	4.E-01	3.E-04	2.E-04	1.E-02	9.E-05			2.E-05	2.E-01	4.E-01	3.E-03	1.E-02	1.E-01	1.E-03
	N		40	40	40	38	38	40	40			38	36	36	36	36	38	38
(Hg)_{HCl} (%)	CC			0.25	0.16	0.38	- 0.44	0.31	0.28	(Hg)_{KOH} (%)			- 0.02	- 0.10	0.38	- 0.28	0.15	0.33
	P			1.E-01	3.E-01	2.E-02	6.E-03	5.E-02	8.E-02				9.E-01	6.E-01	2.E-02	1.E-01	4.E-01	4.E-02
	N			40	40	38	38	40	40				36	36	36	36	38	38
[Fe]_{HCl} (mg g⁻¹)	CC				0.69	0.34	- 0.33	0.16	0.24	[Fe]_{KOH} (mg g⁻¹)				0.60	0.62	- 0.38	- 0.15	0.48
	P				8.E-07	4.E-02	4.E-02	3.E-01	1.E-01					1.E-04	1.E-04	2.E-02	4.E-01	3.E-03
	N				40	38	38	40	40					36	34	34	36	36
[Al]_{HCl} (mg g⁻¹)	CC					0.57	- 0.42	0.12	0.39	[Al]_{KOH} (mg g⁻¹)					0.68	- 0.48	0.16	0.50
	P					2.E-04	9.E-03	5.E-01	1.E-02						1.E-05	4.E-03	4.E-01	2.E-03
	N					38	38	40	40						34	34	36	36
Clay (g/100g)	CC						- 0.80	0.37	0.80	Clay (g/100g)						- 0.80	0.37	0.80
	P						3.E-09	2.E-02	2.E-09							3.E-09	2.E-02	2.E-09
	N						38	38	38							38	38	38
Silt (g/100g)	CC							- 0.57	- 0.70	Silt (g/100g)							- 0.57	- 0.70
	P							2.E-04	1.E-06								2.E-04	1.E-06
	N							38	38								38	38
C (g/100g)	CC								0.47	C (g/100g)								0.47
	P								0.00251									3.E-03
	N								40									40

Table 1b

	Stati	[Hg] _{Asco} (µg g ⁻¹)	(Hg) _{Asco} (%)	[Fe] _{Asco} (mg g ⁻¹)	[Al] _{Asco} (mg g ⁻¹)	Clay (g/100g)	Silt (g/100g)	C (g/100g)	S (g/100g)		[Hg] _{NH4OH} (µg g ⁻¹)	(Hg) _{NH4OH} (%)	[Fe] _{NH4OH} (mg g ⁻¹)	[Al] _{NH4OH} (mg g ⁻¹)	Clay (g/100g)	Silt (g/100g)	C (g/100g)	S (g/100g)
[HgT] (µg g⁻¹)	CC	0.77	0.21	0.40	0.35	0.59	- 0.60	0.42	0.62	[HgT] (µg g⁻¹)	0.90	0.45	0.27	0.08	0.59	- 0.60	0.42	0.62
	P	1.E-08	2.E-01	1.E-02	3.E-02	9.E-05	7.E-05	7.E-03	2.E-05		2.E-15	4.E-03	1.E-01	6.E-01	9.E-05	7.E-05	7.E-03	2.E-05
	N	39	39	40	40	38	38	40	40		40	40	39	40	38	38	40	40
[Hg]_{Asco} (µg g⁻¹)	CC		0.73	0.68	0.60	0.64	- 0.66	0.56	0.59	[Hg]_{NH4OH} (µg g⁻¹)		0.74	0.31	0.08	0.70	- 0.70	0.65	0.71
	P		2.E-07	2.E-06	5.E-05	2.E-05	9.E-06	2.E-04	8.E-05			4.E-08	6.E-02	6.E-01	1.E-06	9.E-07	7.E-06	3.E-07
	N		39	39	39	37	37	39	39			40	39	40	38	38	40	40
(Hg)_{Asco} (%)	CC			0.62	0.51	0.39	- 0.35	0.37	0.32	(Hg)_{NH4OH} (%)			0.23	0.06	0.68	- 0.68	0.67	0.67
	P			3.E-05	9.E-04	2.E-02	4.E-02	2.E-02	4.E-02				2.E-01	7.E-01	3.E-06	3.E-06	2.E-06	2.E-06
	N			39	39	37	37	39	39				39	40	38	38	40	40
[Fe]_{Asco} (mg g⁻¹)	CC				0.98	0.42	- 0.52	0.30	0.37	[Fe]_{NH4OH} (mg g⁻¹)				0.64	0.06	- 0.24	0.23	0.15
	P				3.E-27	8.E-03	7.E-04	6.E-02	2.E-02					1.E-05	7.E-01	2.E-01	2.E-01	4.E-01
	N				40	38	38	40	40					39	37	37	39	39
[Al]_{Asco} (mg g⁻¹)	CC					0.37	- 0.47	0.22	0.31	[Al]_{NH4OH} (mg g⁻¹)					- 0.01	- 0.22	0.06	- 0.07
	P					2.E-02	3.E-03	2.E-01	5.E-02						9.E-01	2.E-01	7.E-01	7.E-01
	N					38	38	40	40						38	38	40	40
Clay (g/100g)	CC						- 0.80	0.37	0.80	Clay (g/100g)						- 0.80	0.37	0.80
	P						3.E-09	2.E-02	2.E-09							3.E-09	2.E-02	2.E-09
	N						38	38	38							38	38	38
Silt (g/100g)	CC							- 0.57	- 0.70	Silt (g/100g)							- 0.57	- 0.70
	P							2.E-04	1.E-06								2.E-04	1.E-06
	N							38	38								38	38
C (g/100g)	CC								0.47	C (g/100g)								0.47
	P								3.E-03									3.E-03
	N								40									40

Table 2: Pearson correlation matrix (correlation coefficient (CC), P value (P) and number of samples (N)) of contaminated soils extracted Hg, Hg extraction yields, Fe, Al, Clay size fraction, Fine silts, C and S for total and (a) HCl/HNO₃ (labeled HCl) and ascorbate (labeled Asco) selective extractions, and (b) KOH and NH₄OH selective extractions.

Table 2a

	Stati	[Hg] _{HCl} (µg g ⁻¹)	(Hg) _{HCl} (%)	[Fe] _{HCl} (mg g ⁻¹)	[Al] _{HCl} (mg g ⁻¹)	Clay (g/100g)	Sand (g/100g)	C (g/100g)	S (g/100g)		[Hg] _{KOH} (µg g ⁻¹)	(Hg) _{KOH} (%)	[Fe] _{KOH} (mg g ⁻¹)	[Al] _{KOH} (mg g ⁻¹)	Clay (g/100g)	Sand (g/100g)	C (g/100g)	S (g/100g)
[HgT] (µg g⁻¹)	CC	1.00	0.22	- 0.29	- 0.34	- 0.52	0.50	- 0.09	- 0.08	[HgT] (µg g⁻¹)	0.88	0.22	- 0.21	- 0.38	- 0.52	0.50	- 0.09	- 0.08
	P	4.E-86	2.E-01	8.E-02	4.E-02	1.E-03	2.E-03	6.E-01	7.E-01		2.E-12	2.E-01	2.E-01	2.E-02	1.E-03	2.E-03	6.E-01	7.E-01
	N	37	37	37	37	37	37	37	37		35	35	37	37	37	37	37	37
[Hg]_{HCl} (µg g⁻¹)	CC		0.22	- 0.30	- 0.35	- 0.52	0.50	- 0.09	- 0.08	[Hg]_{KOH} (µg g⁻¹)		0.55	- 0.20	- 0.29	- 0.46	0.52	- 0.27	- 0.25
	P		2.E-01	8.E-02	4.E-02	1.E-03	2.E-03	6.E-01	7.E-01			7.E-04	3.E-01	9.E-02	6.E-03	1.E-03	1.E-01	1.E-01
	N		37	37	37	37	37	37	37			35	35	35	35	35	35	35
(Hg)_{HCl} (%)	CC			- 0.50	- 0.80	- 0.14	0.22	0.21	0.19	(Hg)_{KOH} (%)			0.01	0.18	- 0.04	0.26	- 0.40	- 0.34
	P			2.E-03	3.E-09	4.E-01	2.E-01	2.E-01	3.E-01				9.E-01	3.E-01	8.E-01	1.E-01	2.E-02	4.E-02
	N			37	37	37	37	37	37				35	35	35	35	35	35
[Fe]_{HCl} (mg g⁻¹)	CC				0.86	0.37	- 0.32	- 0.14	- 0.08	[Fe]_{KOH} (mg g⁻¹)				0.54	0.37	- 0.29	0.00	0.04
	P				8.E-12	3.E-02	5.E-02	4.E-01	6.E-01					6.E-04	3.E-02	8.E-02	1.E+00	8.E-01
	N				37	37	37	37	37					37	37	37	37	37
[Al]_{HCl} (mg g⁻¹)	CC					0.42	- 0.41	- 0.11	- 0.07	[Al]_{KOH} (mg g⁻¹)					0.57	- 0.49	0.09	0.22
	P					1.E-02	1.E-02	5.E-01	7.E-01						2.E-04	2.E-03	6.E-01	2.E-01
	N					37	37	37	37						37	37	37	37
Clay (g/100g)	CC						- 0.85	0.05	0.09	Clay (g/100g)						- 0.85	0.05	0.09
	P						4.E-11	8.E-01	6.E-01							4.E-11	8.E-01	6.E-01
	N						37	37	37							37	37	37
Sand (g/100g)	CC							- 0.38	- 0.41	Sand (g/100g)							- 0.38	- 0.41
	P							2.E-02	1.E-02								2.E-02	1.E-02
	N							37	37								37	37
C (g/100g)	CC								0.94	C (g/100g)								0.94
	P								2.1E-18									2.E-18
	N								37									37

Table 2b

	Statist	[Hg] _{Asco} (μg g ⁻¹)	(Hg) _{Asco} (%)	[Fe] _{Asco} (mg g ⁻¹)	[Al] _{Asco} (mg g ⁻¹)	Clay (g/100g)	Sand (g/100g)	C (g/100g)	S (g/100g)		[Hg] _{NH4OH} (μg g ⁻¹)	(Hg) _{NH4OH} (%)	[Fe] _{NH4OH} (mg g ⁻¹)	[Al] _{NH4OH} (mg g ⁻¹)	Clay (g/100g)	Sand (g/100g)	C (g/100g)	S (g/100g)
[HgT] (μg g ⁻¹)	CC	0.89	- 0.23	- 0.27	- 0.40	- 0.52	0.50	- 0.09	- 0.08	[HgT] (μg g ⁻¹)	0.96	0.10	- 0.15	- 0.27	- 0.52	0.50	- 0.09	- 0.08
	P	1.E-13	2.E-01	1.E-01	2.E-02	1.E-03	2.E-03	6.E-01	7.E-01		7.E-21	5.E-01	4.E-01	1.E-01	1.E-03	2.E-03	6.E-01	7.E-01
	N	37	37	36	36	37	37	37	37		37	37	37	37	37	37	37	37
[Hg] _{Asco} (μg g ⁻¹)	CC	0.12	- 0.34	- 0.45	- 0.53	0.48	0.04	0.02		[Hg] _{NH4OH} (μg g ⁻¹)	0.31	- 0.18	- 0.25	- 0.50	0.53	- 0.15	- 0.13	
	P	5.E-01	4.E-02	6.E-03	8.E-04	3.E-03	8.E-01	9.E-01			6.E-02	3.E-01	1.E-01	1.E-03	8.E-04	4.E-01	4.E-01	
	N	37	36	36	37	37	37	37			37	37	37	37	37	37	37	
(Hg) _{Asco} (%)	CC		- 0.26	- 0.00	0.25	- 0.25	0.39	0.35		(Hg) _{NH4OH} (%)		- 0.08	0.14	- 0.02	0.18	- 0.13	- 0.05	
	P		1.E-01	1.E+00	1.E-01	1.E-01	2.E-02	3.E-02			7.E-01	4.E-01	9.E-01	3.E-01	5.E-01	8.E-01		
	N		36	36	37	37	37	37			37	37	37	37	37	37		
[Fe] _{Asco} (mg g ⁻¹)	CC				0.85	0.30	- 0.32	- 0.10	- 0.03	[Fe] _{NH4OH} (mg g ⁻¹)				0.41	0.37	- 0.32	0.47	0.43
	P				8.E-11	8.E-02	6.E-02	6.E-01	9.E-01			1.E-02	2.E-02	5.E-02	3.E-03	7.E-03		
	N				36	36	36	36			37	37	37	37	37			
[Al] _{Asco} (mg g ⁻¹)	CC					0.56	- 0.53	0.06	0.17	[Al] _{NH4OH} (mg g ⁻¹)				0.46	- 0.44	0.23	0.33	
	P					4.E-04	8.E-04	7.E-01	3.E-01			4.E-03	7.E-03	2.E-01	5.E-02			
	N					36	36	36			37	37	37	37				
Clay (g/100g)	CC						- 0.85	0.05	0.09	Clay (g/100g)					- 0.85	0.05	0.09	
	P						4.E-11	8.E-01	6.E-01						4.E-11	8.E-01	6.E-01	
	N						37	37	37						37	37	37	
Sand (g/100g)	CC							- 0.38	- 0.41	Sand (g/100g)						- 0.38	- 0.41	
	P							2.E-02	1.E-02						2.E-02	1.E-02		
	N							37	37						37	37		
C (g/100g)	CC								0.94	C (g/100g)							0.94	
	P								2.E-18							2.E-18		
	N								37							37		

Figure captions

Fig. 1: Top left: french Guiana map with the studied site location (closed circle). Right and bottom: detailed map of the studied site, including general watershed scheme with soil sampling locations, and associated legend.

Fig. 2: Evolutions with depth of total Hg, C and C/N ratio for (a) pristine and (b) contaminated soils. Evolutions with depth of the clay- and sand-size fractions are reported for pristine and contaminated soils, respectively.

Fig. 3: XRD patterns normalized on quartz peak (refer to the text for details) for raw samples, and following ascorbate, KOH, NH_4OH and HCl/HNO_3 extractions.

Fig. 4: Top : Evolutions with depth of Fe and Al concentrations extracted by ascorbate and corresponding Al/Fe ratio. Bottom: same graphs as top, focused on calculated crystalline + residual fraction in pristine soils.

Fig. 5: Evolutions with depth of $(\text{Hg})_{\text{HCl}/\text{HNO}_3}$, $(\text{Hg})_{\text{CR}}$, $(\text{Hg})_{\text{Asco}}$, $(\text{Hg})_{\text{NH}_4\text{OH}}$, and $(\text{Hg})_{\text{KOH}}$ extraction yield (%) in pristine soils. Triangles, circles and squares refer to toposequence I, II and III, and white, grey and black filled colours refer to ferralsols, acrisols and gleysols, respectively.

Fig. 6: XRD patterns of nodules from pristine soils I-2 (10-20cm), I-2 (30-40cm), and I-2 (180-200cm).

Fig. 7: μXRF mapping of Si, K, Fe, Au and Hg of SL6 (30-50 cm) sample and counts measured on $\text{L}\alpha$ edge fluorescence of Hg and Au versus $\text{K}\alpha$ radiation of Si, K and Fe, and comparison on counts measured for Hg (Y axis) versus Au (X axis).

Fig. 8: Evolution with depth of $(\text{Hg})_{\text{HCl}/\text{HNO}_3}$, $(\text{Hg})_{\text{CR}}$, $(\text{Hg})_{\text{Asco}}$, $(\text{Hg})_{\text{NH}_4\text{OH}}$, $(\text{Hg})_{\text{KOH}}$ and (Hg^0) pyrolysis extraction yields (%) in contaminated soils.

Fig. 1.

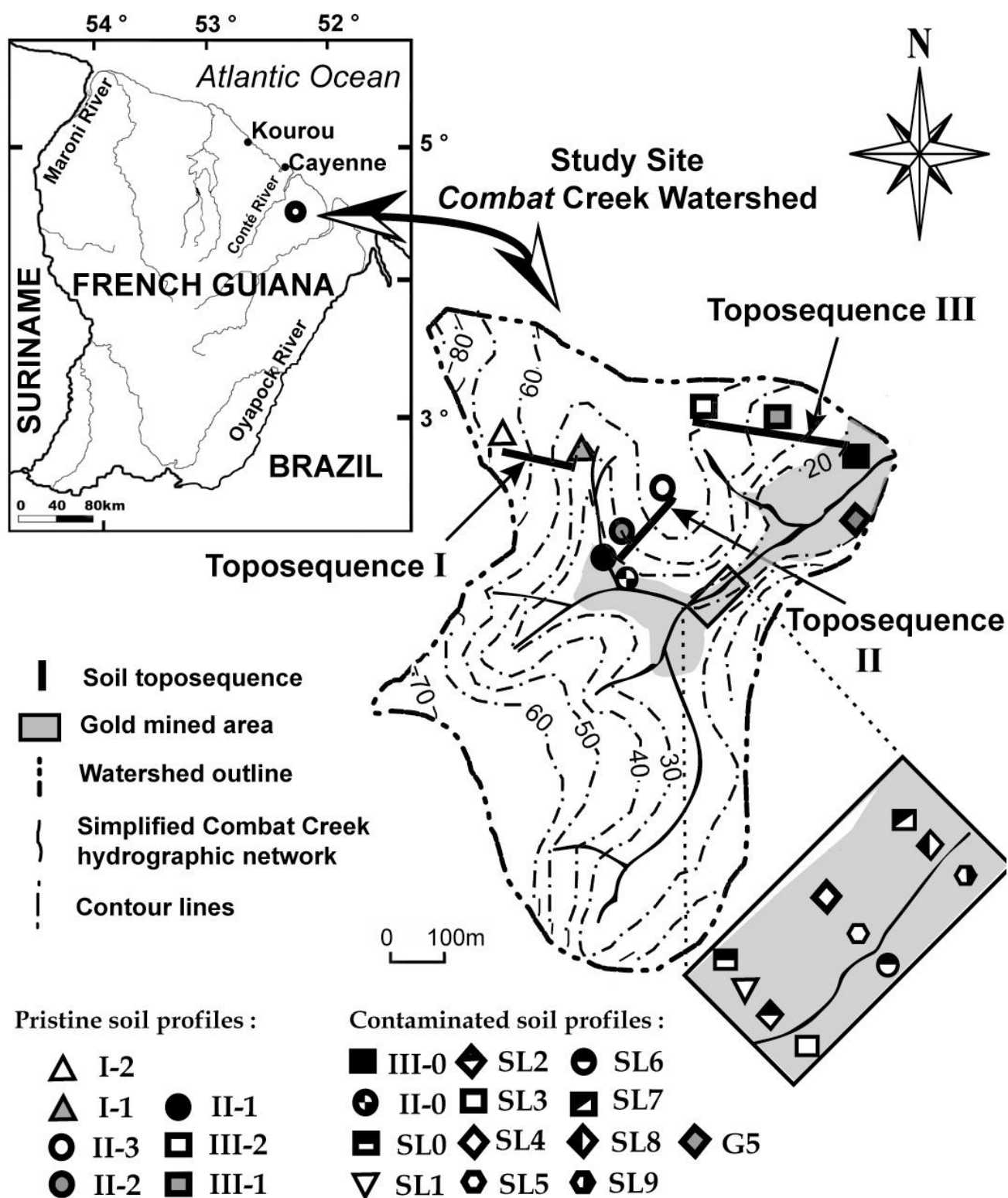


Fig. 2.a.

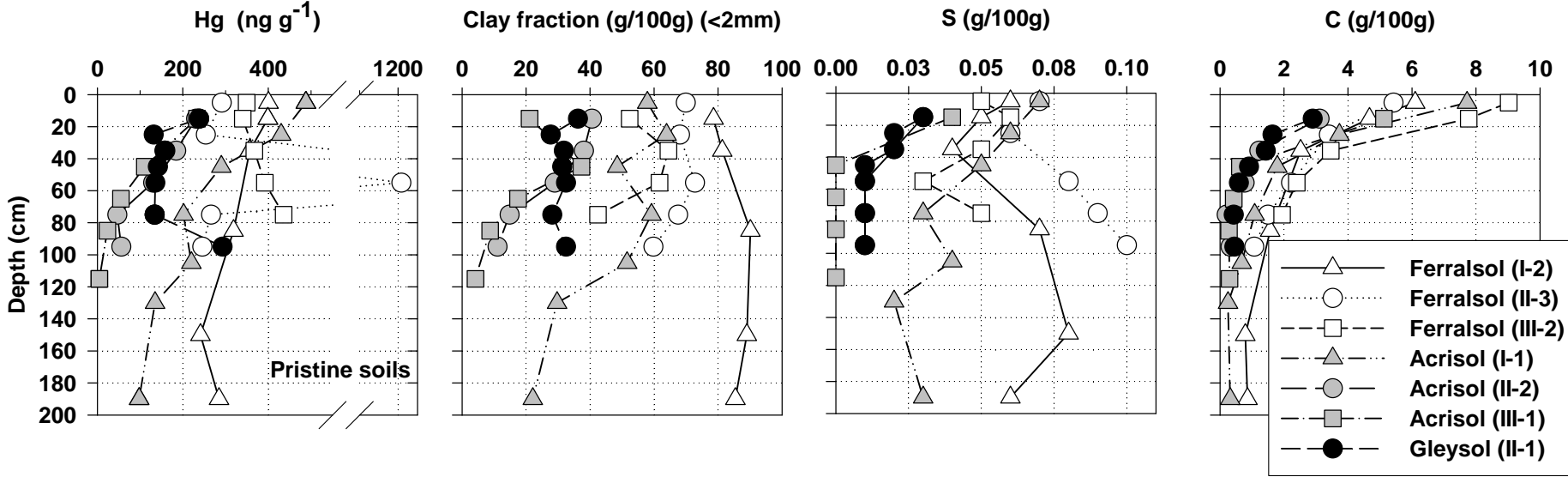


Fig. 2.b.

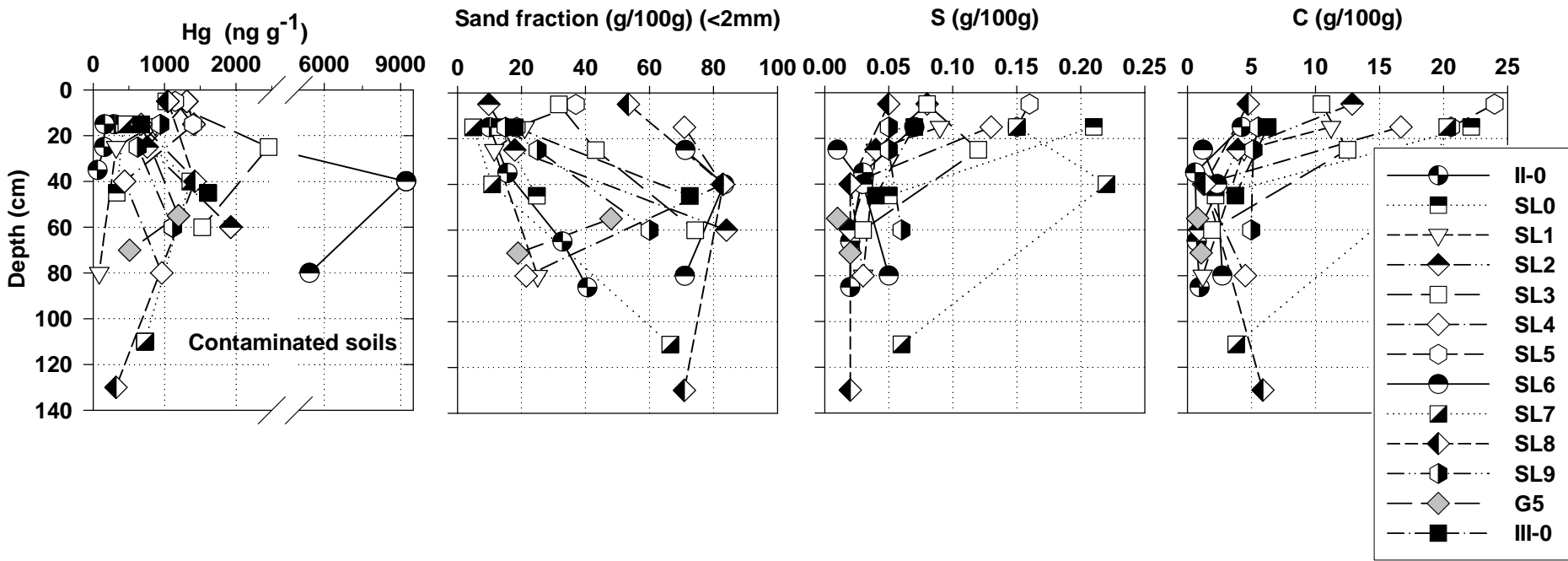


Fig. 3.

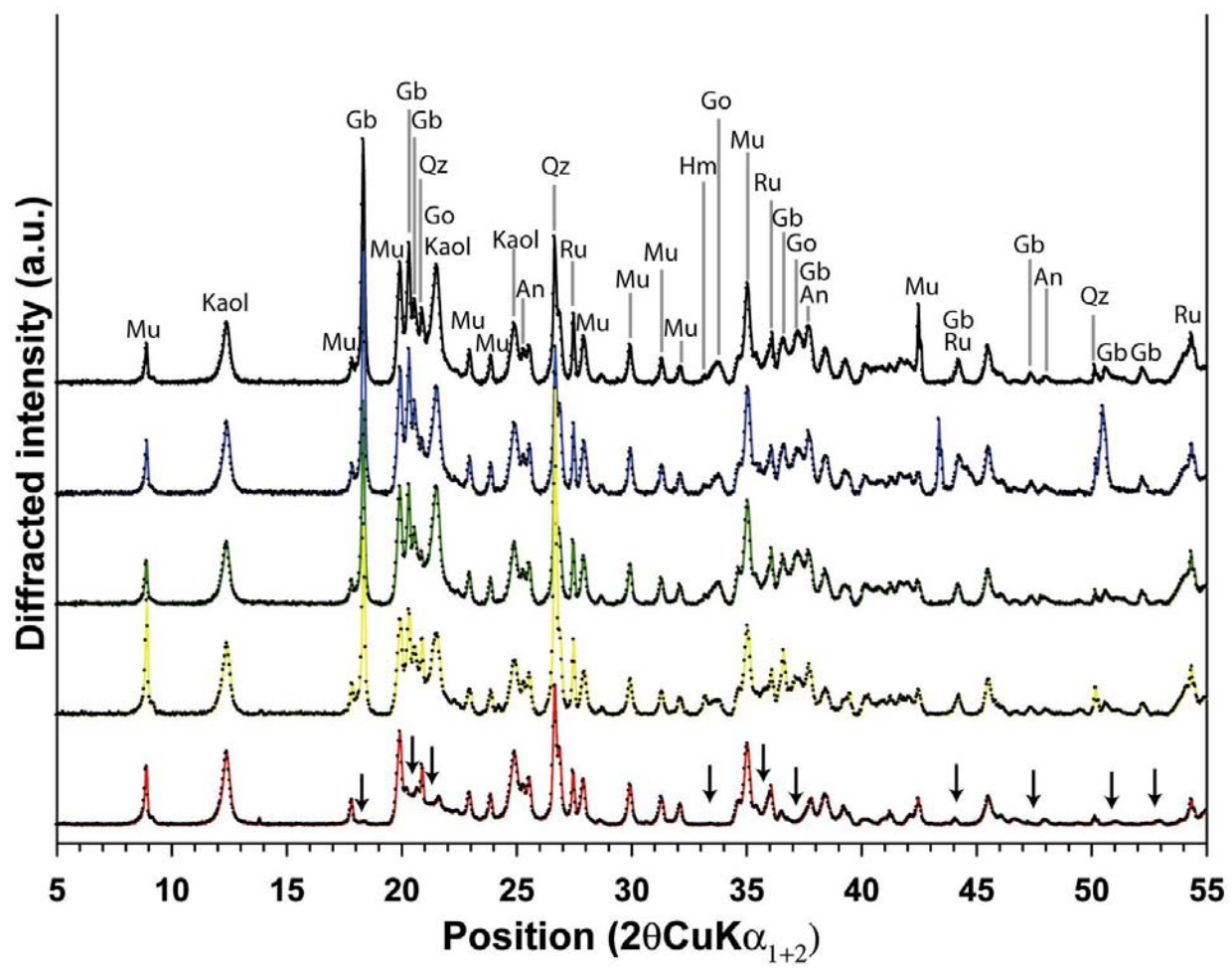


Fig. 4.

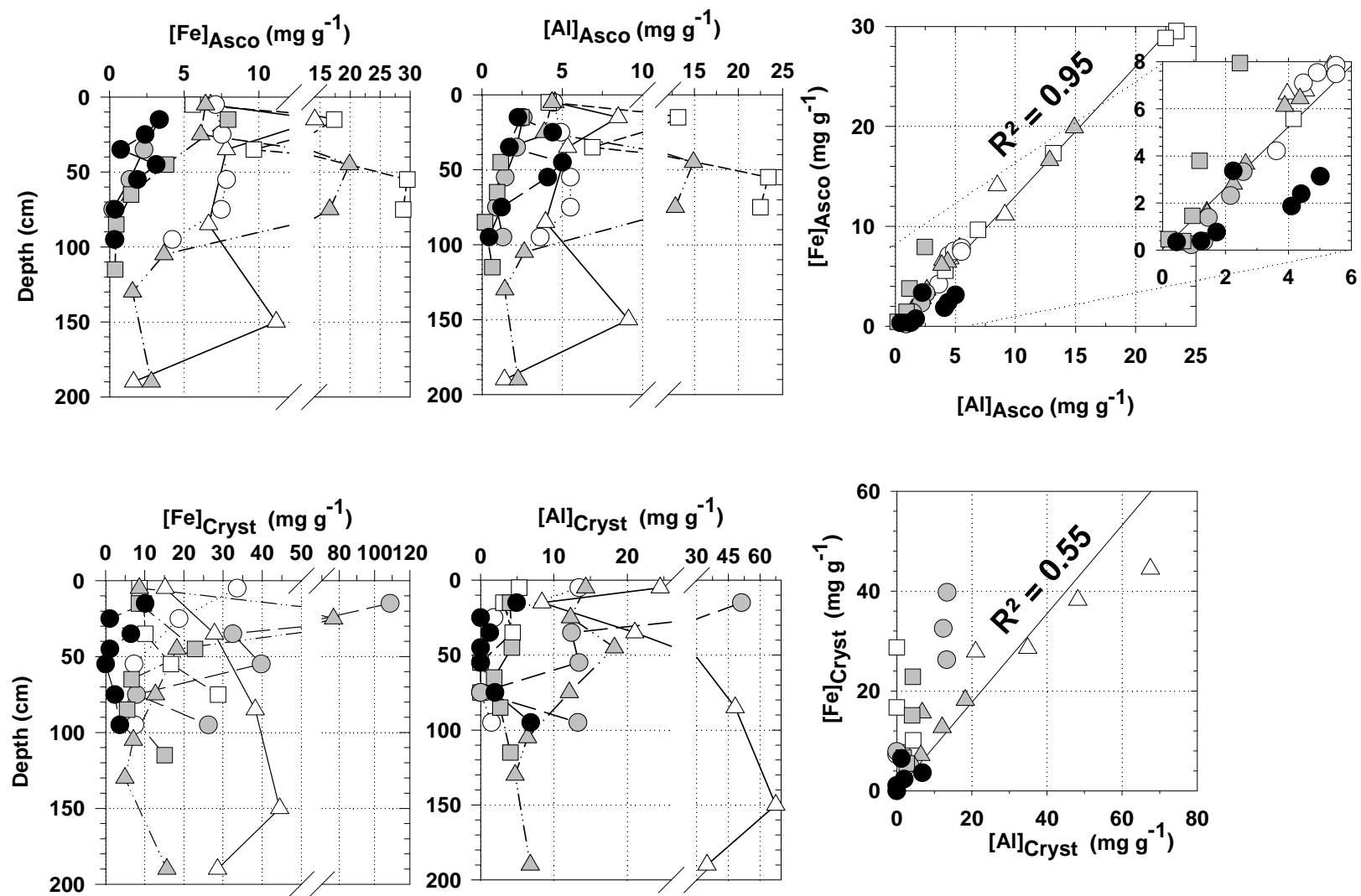


Fig. 5.

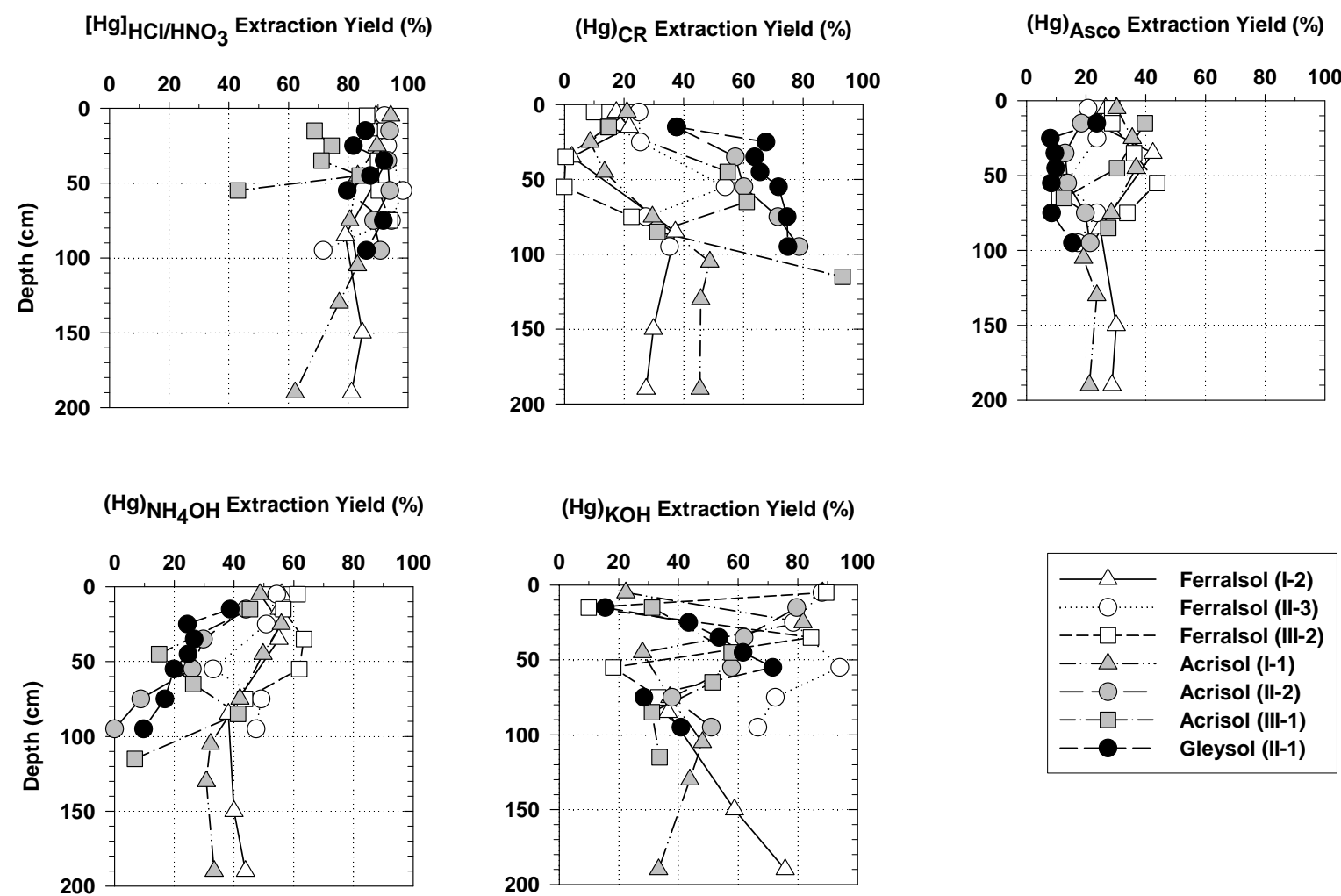


Fig. 6.

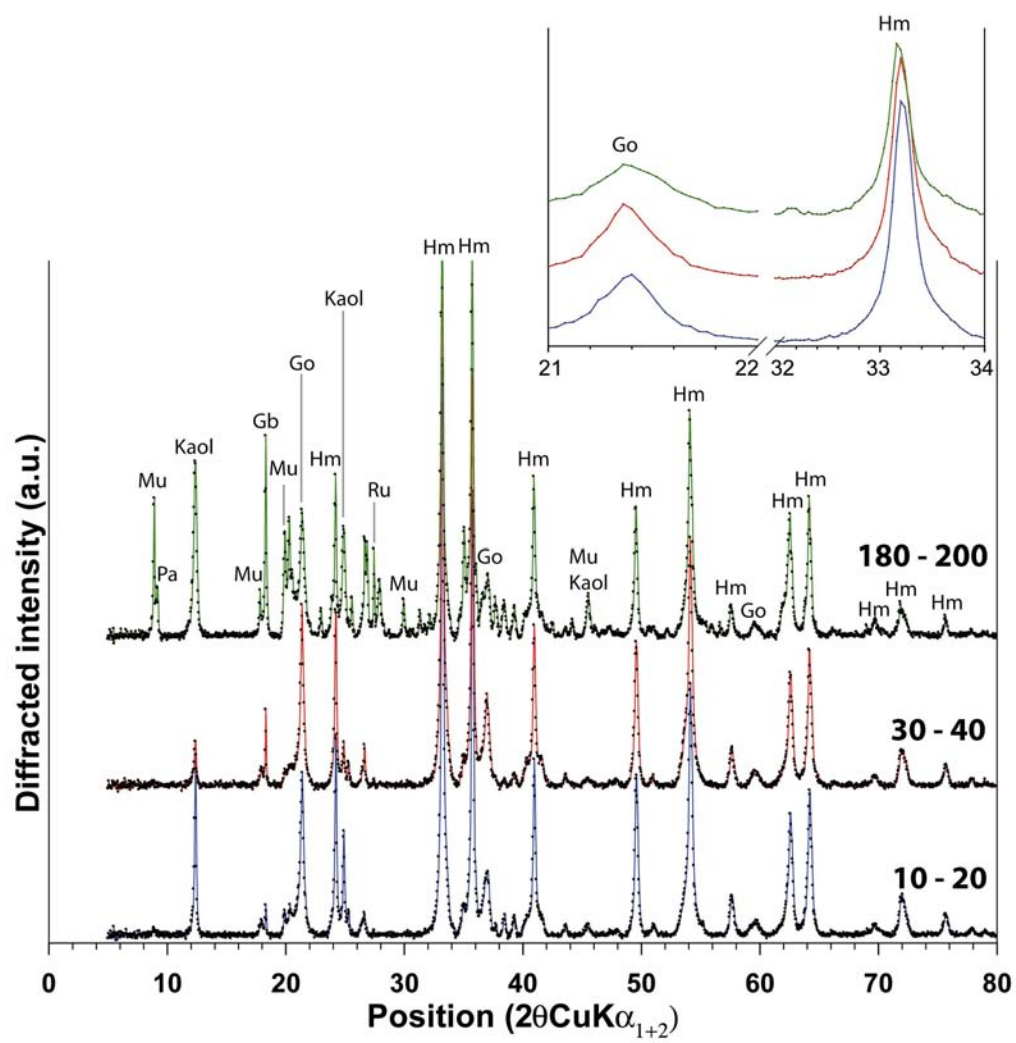


Fig . 7.

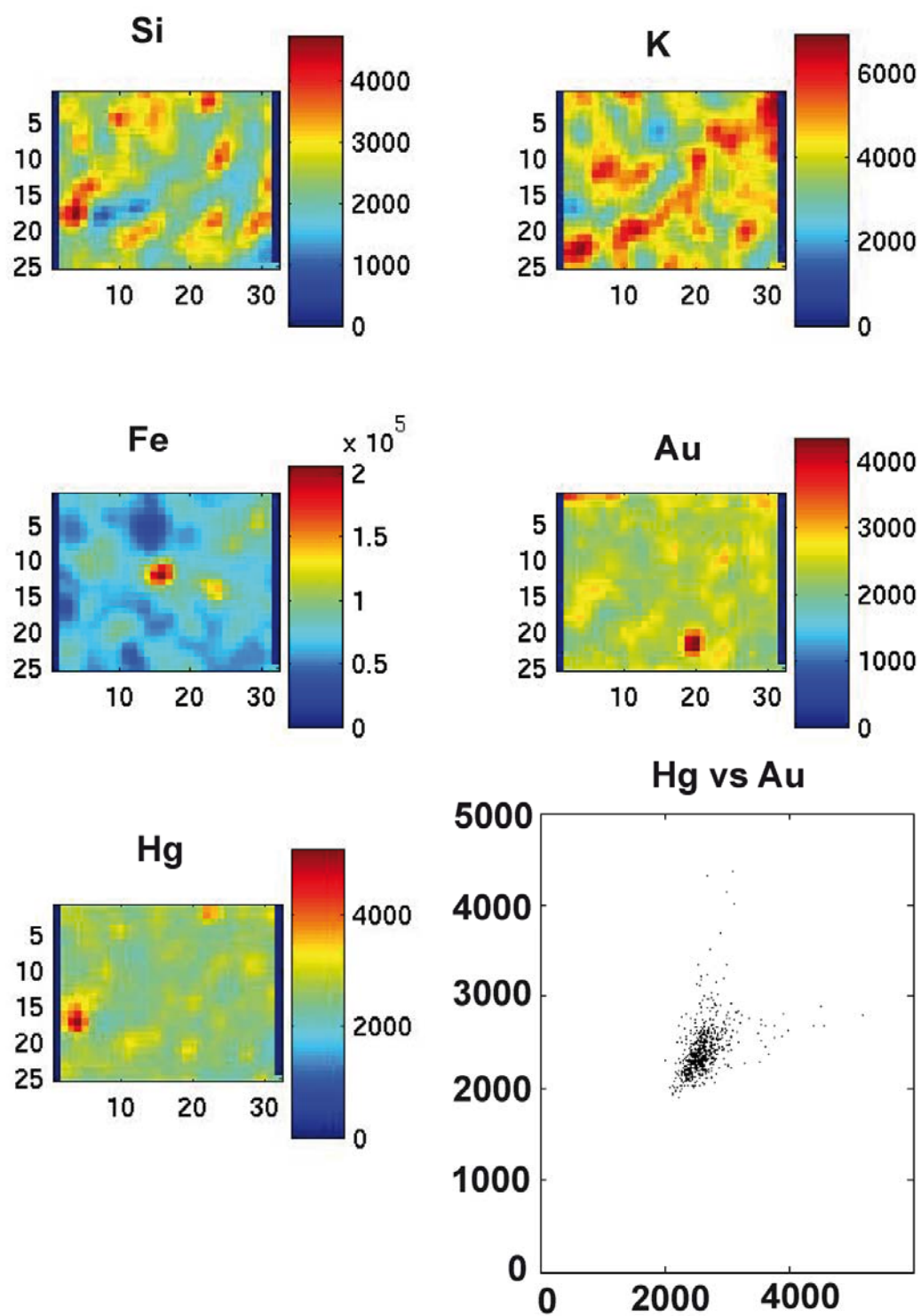
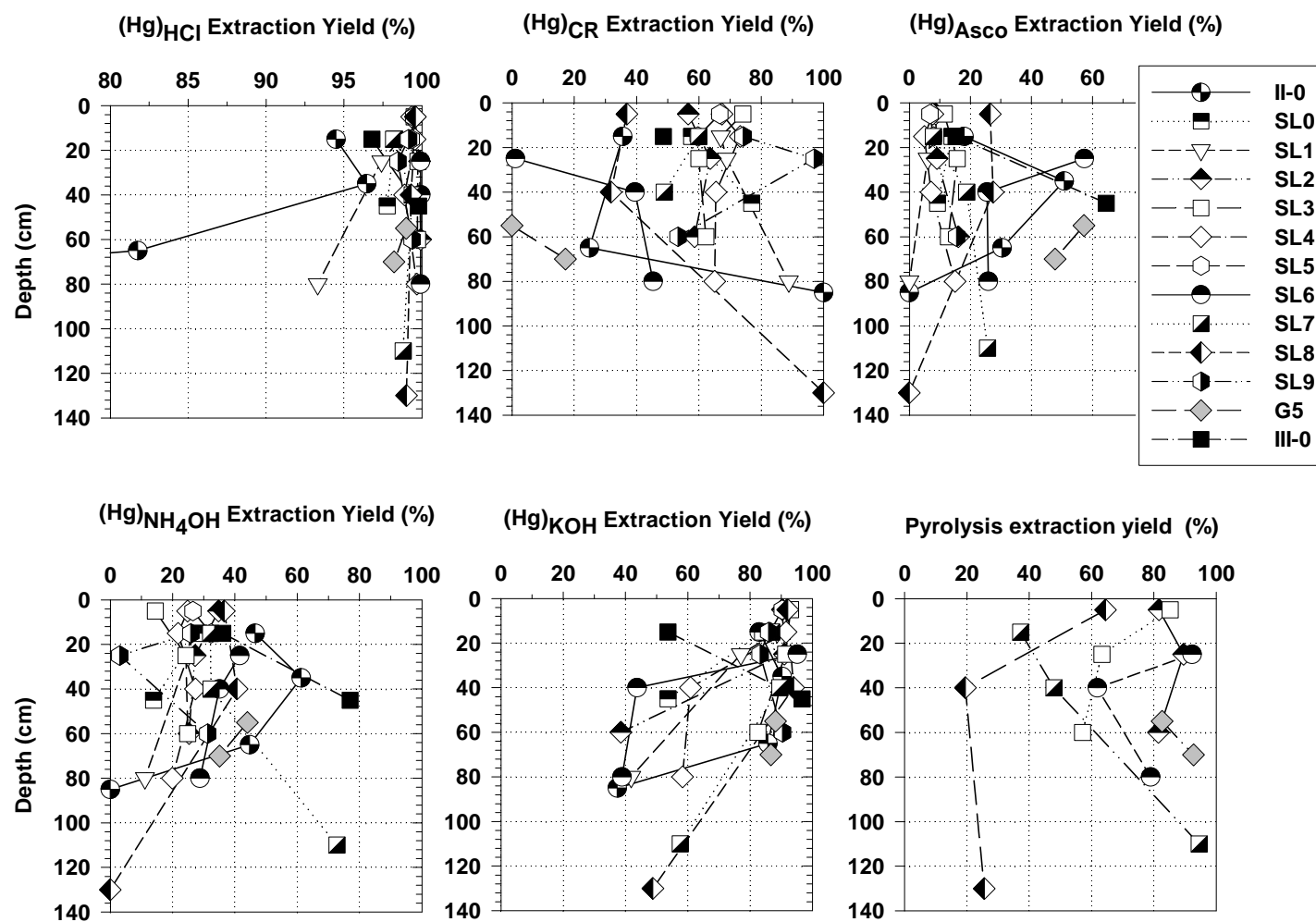


Fig . 8.



Supplementary data 2

(Electronic table)

Table E1: Percent recoveries of Hg in supernatant and solid residue for Certified materials CRM 7002, MESS-3 and sample I-1 (0-10 cm) for ascorbate, NH₄OH , KOH and HCl/HNO₃ selective extractions.

	Ascorbate			NH ₄ OH		KOH			HCl/HNO ₃		
Sample	CRM 7002	MESS- 3	I-1 (0-10 cm)	CRM 7002	MESS- 3	CRM 7002	MESS- 3	I-1 (0-10 cm)	CRM 7002	MESS- 3	I-1 (0-10 cm)
Mean	98.8	68.7	60.4	102.1	93.5	106.5	96.4	87.9	101.0	114.9	109.5
Std. Error	12.3	13.4	5.31	9.57	10.9	13.6	5.45	3.27	6.46	19.1	9.70
Median	89.9	62.9	60.4	99.0	88.2	94.5	96.5	90.4	96.7	95.6	108.5
0.25 Perc.	75.5	55.6	53.5	90.3	80.4	90.5	89.3	83.7	96.7	91.0	95.7
0.75 Perc.	116.2	77.8	67.3	114.8	107.9	117.8	103.5	91.5	110.7	127.6	123.3
Size (N)	6	5	3	3	3	5	3.0	3	7	5	4

Supplementary Figure captions

Fig. E1a: X-ray diffraction pattern of CRM Mess-3 (black trace) showing identified minerals (colored ticks)

Fig. E1b: Normalized X-ray diffraction patterns of CRM Mess-3 before and after NH_4OH extraction (black and red traces, respectively) showing identified minerals (colored ticks)

Fig. E1c: Normalized X-ray diffraction patterns of CRM Mess-3 before and after KOH extraction (black and red traces, respectively) showing identified minerals (colored ticks)

Fig. E1d: Normalized X-ray diffraction patterns of CRM Mess-3 before and after ascorbate extraction (black and red traces, respectively) showing identified minerals (colored ticks)

Fig. E1e: Normalized X-ray diffraction patterns of CRM Mess-3 before and after HCl/HNO_3 extraction (black and red traces, respectively) showing identified minerals (colored ticks)

Fig. E2a: X-ray diffraction pattern of CRM 7002 (black trace) showing identified minerals (colored ticks)

Fig. E2b: Normalized X-ray diffraction patterns of CRM 7002 before and after NH_4OH extraction (black and red traces, respectively) showing identified minerals (colored ticks)

Fig. E2c: Normalized X-ray diffraction patterns of CRM 7002 before and after KOH extraction (black and red traces, respectively) showing identified minerals (colored ticks)

Fig. E2d: Normalized X-ray diffraction patterns of CRM 7002 before and after ascorbate extraction (black and red traces, respectively) showing identified minerals (colored ticks)

Fig. E2e: Normalized X-ray diffraction patterns of CRM 7002 before and after HCl/HNO₃ extraction (black and red traces, respectively) showing identified minerals (colored ticks)

Fig. E3a: X-ray diffraction pattern of sample I-1(0-10m) (black trace) showing identified minerals (colored ticks)

Fig. E3b: Normalized X-ray diffraction patterns of sample I-1(0-10m) before and after NH₄OH extraction (black and red traces, respectively) showing identified minerals (colored ticks)

Fig. E3c: Normalized X-ray diffraction patterns of sample I-1(0-10m) before and after KOH extraction (black and red traces, respectively) showing identified minerals (colored ticks)

Fig. E3d: Normalized X-ray diffraction patterns of sample I-1(0-10m) before and after ascorbate extraction (black and red traces, respectively) showing identified minerals (colored ticks)

Fig. E3e: Normalized X-ray diffraction patterns of sample I-1(0-10m) before and after HCl/HNO₃ extraction (black and red traces, respectively) showing identified minerals (colored ticks)

Fig. E4: X-ray diffraction pattern of nodules from sample I-1(180-200m) (black trace) showing identified minerals (colored ticks)

Fig. E5: Total Hg, (Hg)_{HCl/HNO₃}, (Hg)_{residual}, (Hg)_{Asco}, (Hg)_{NH₄OH}, and (Hg)_{KOH} extractions extraction yield (%) vertical profiles in nodules of pristine soils. Triangles refer to toposequence I, triangles up refers to surface nodules, and

triangle down to deeper horizons III. white and grey filled colours refer to oxisol and ultisol, respectively. Filled triangles refer to sol matrix and hair-crossed symbols refer to nodules.

Fig. E1a. X-ray diffraction pattern of CRM Mess-3 (black trace) showing identified minerals (colored ticks)

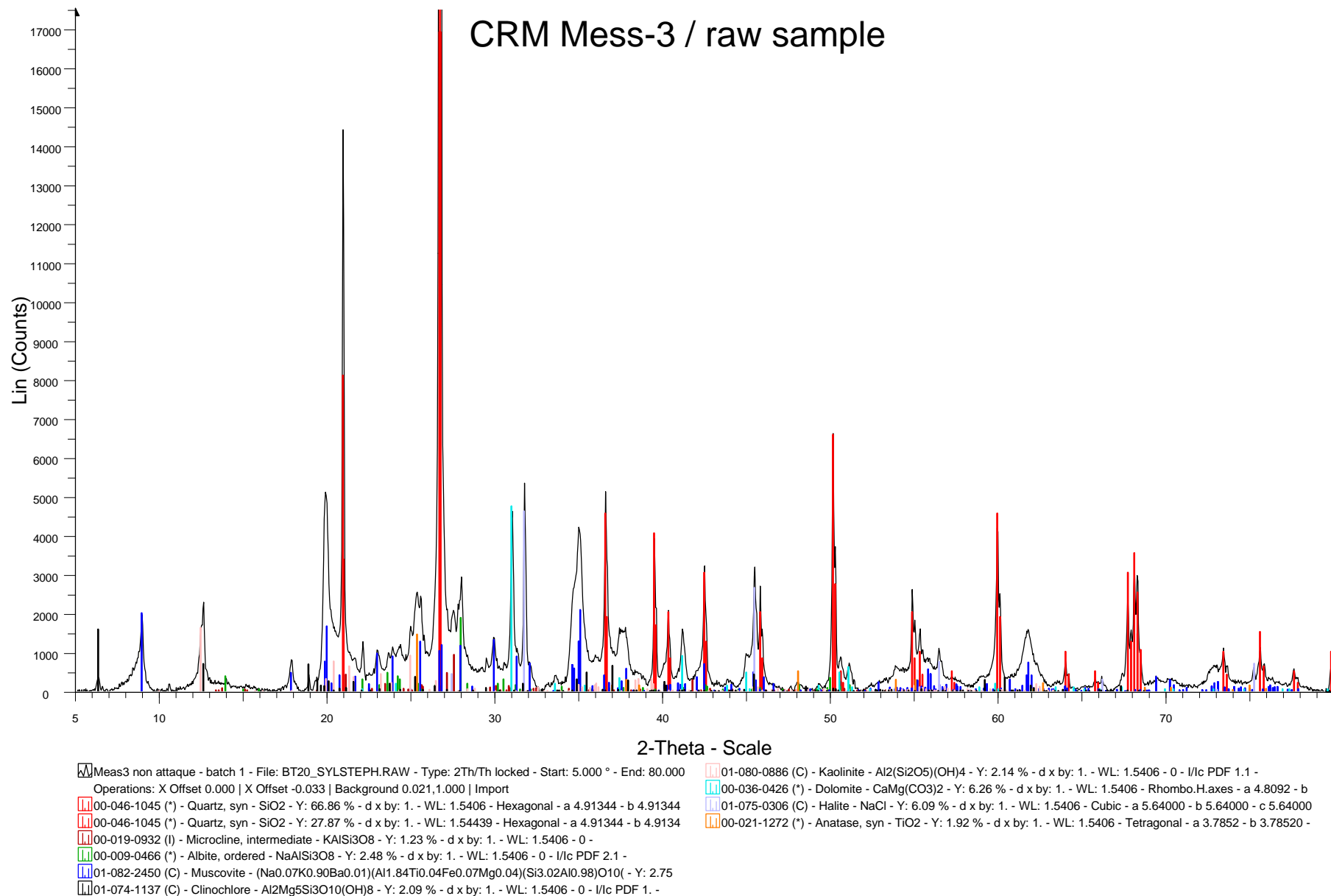


Fig. E1b. Normalized X-ray diffraction patterns of CRM Mess-3 before and after NH_4OH extraction (black and red traces, respectively) showing identified minerals (colored ticks)

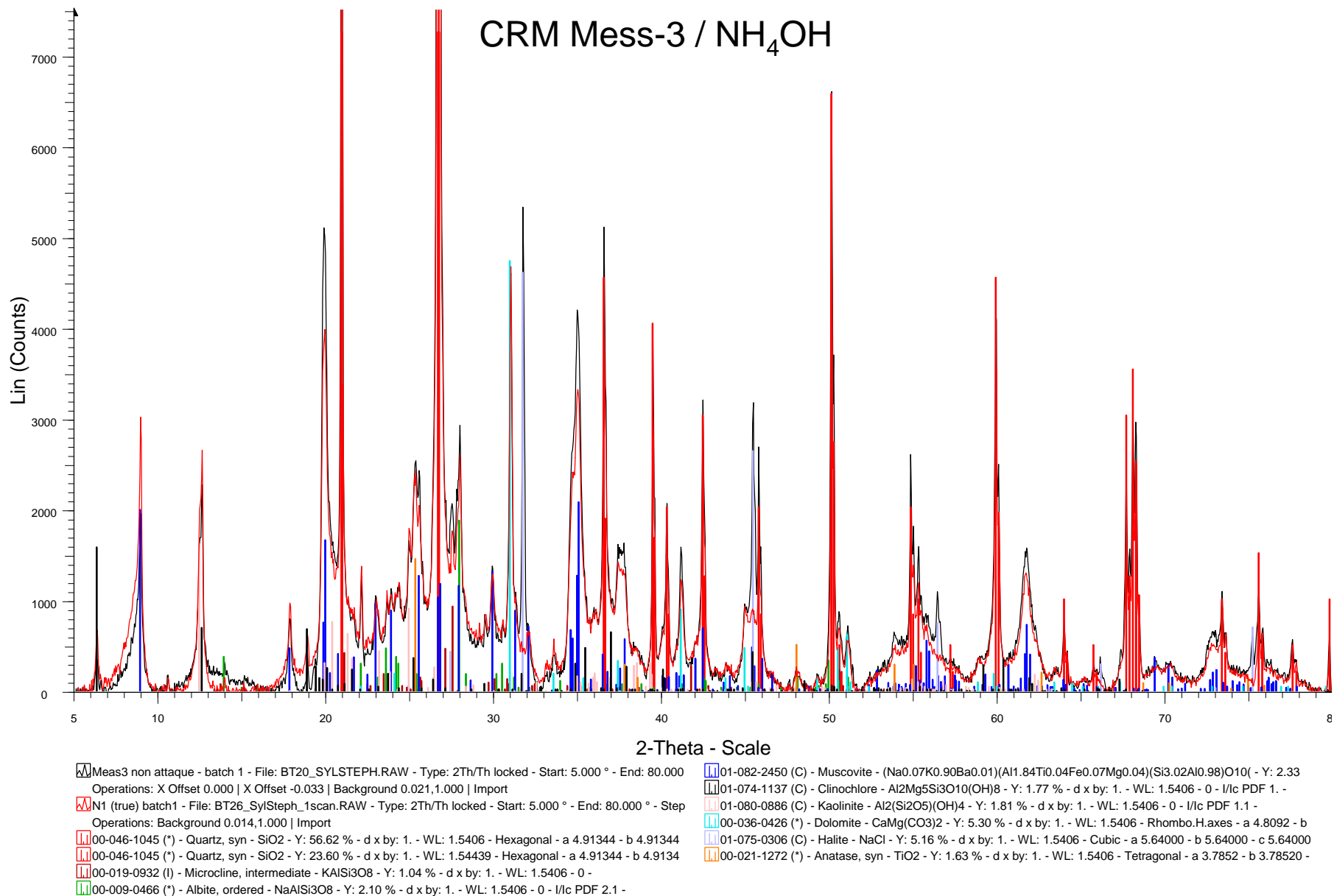


Fig. E1c. Normalized X-ray diffraction patterns of CRM Mess-3 before and after KOH extraction (black and red traces, respectively) showing identified minerals (colored ticks)

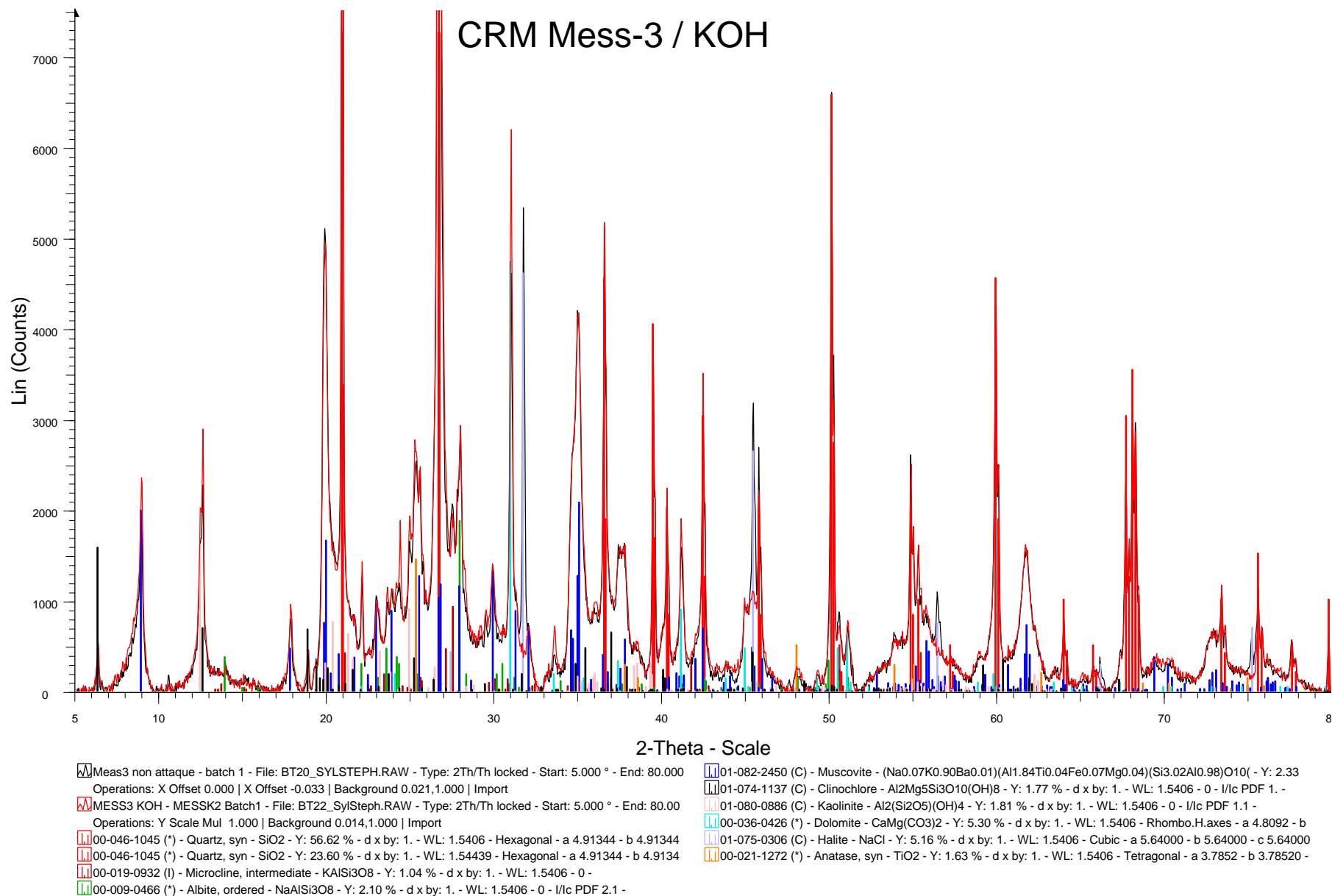


Fig. E1d. Normalized X-ray diffraction patterns of CRM Mess-3 before and after ascorbate extraction (black and red traces, respectively) showing identified minerals (colored ticks)

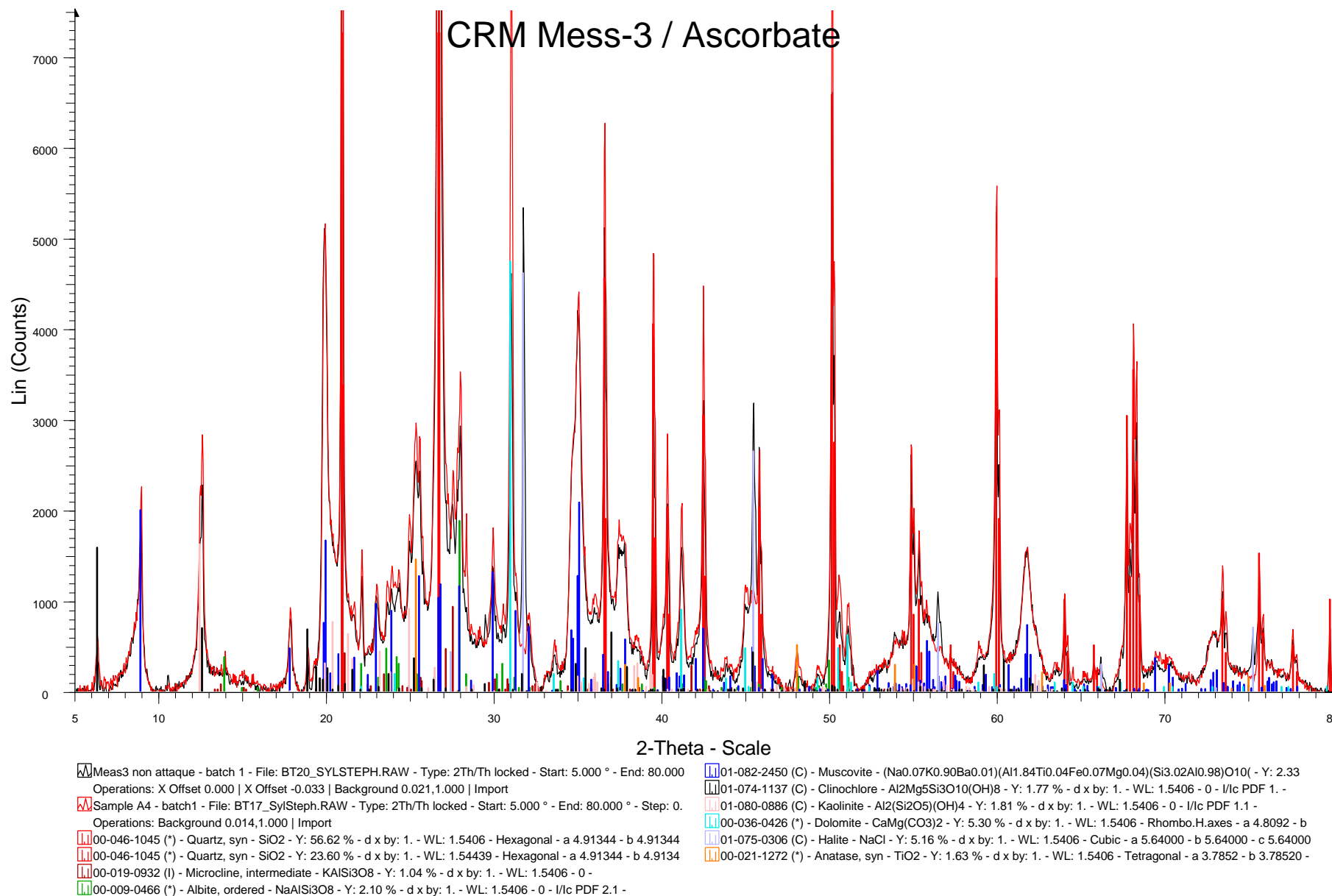


Fig. E1e. Normalized X-ray diffraction patterns of CRM Mess-3 before and after HCl extraction (black and red traces, respectively) showing identified minerals (colored ticks)

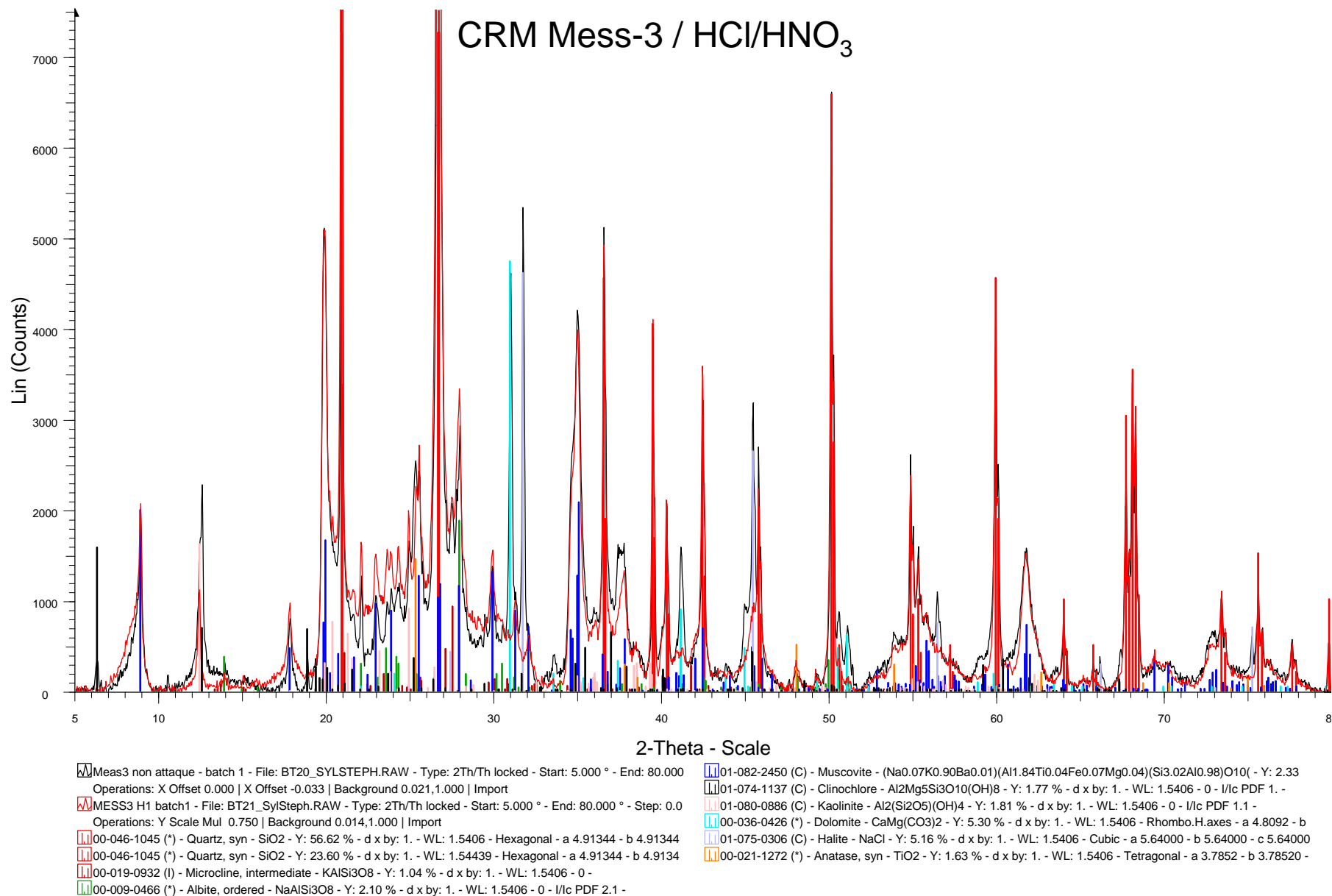


Fig. E2a. X-ray diffraction pattern of CRM 7002 (black trace) showing identified minerals (colored ticks)

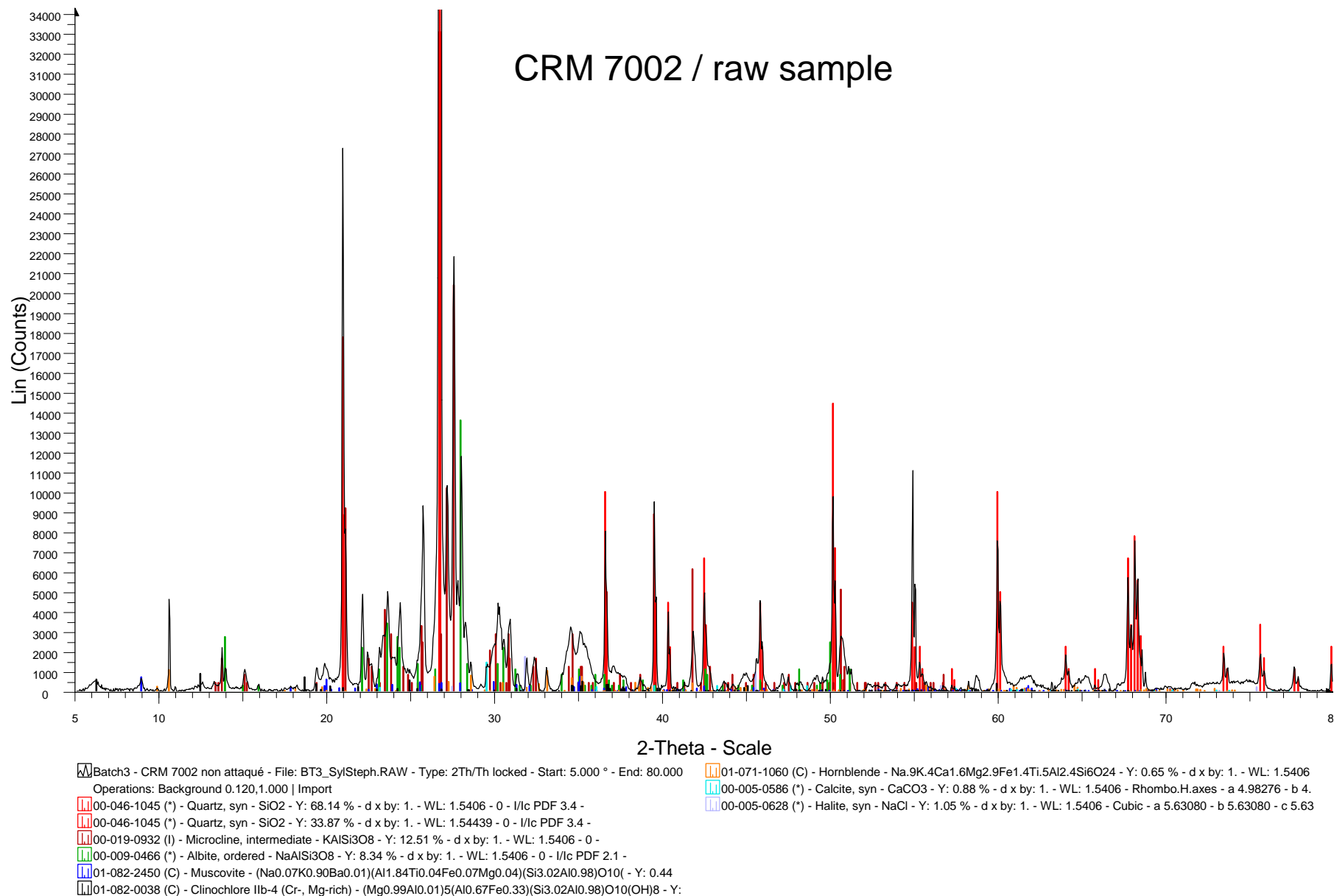
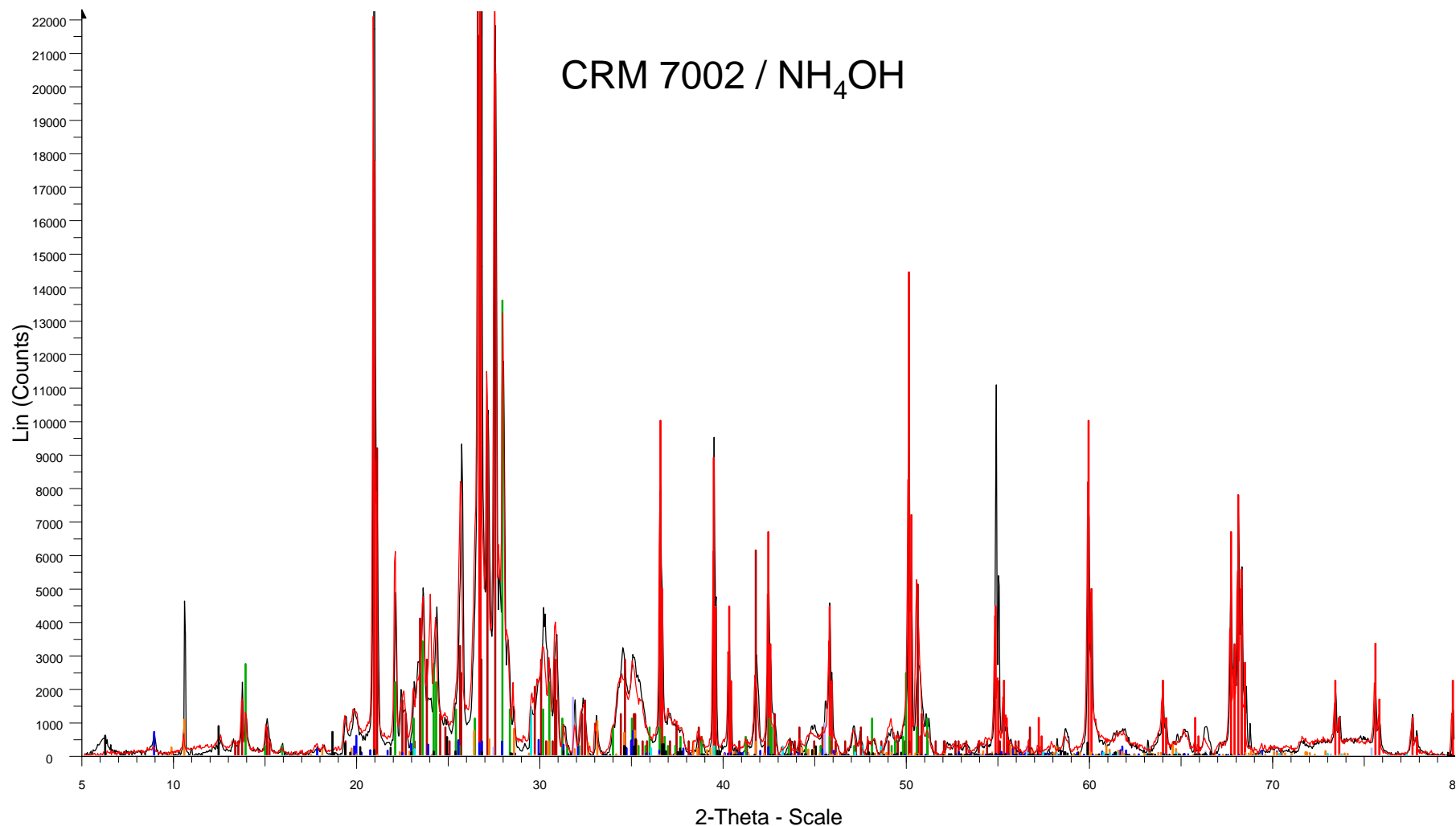


Fig. E2b. Normalized X-ray diffraction patterns of CRM 7002 before and after NH_4OH extraction (black and red traces, respectively) showing identified minerals (colored ticks)



Batch3 - CRM 7002 non attaqué - File: BT3_SylSteph.RAW - Type: 2Th/Th locked - Start: 5.000 ° - End: 80.000
Operations: Background 0.120,1.000 | Import

N2 - Batch1 - File: BT23_SylSteph.RAW - Type: 2Th/Th locked - Start: 5.000 ° - End: 80.000 ° - Step: 0.040 ° -
Operations: Y Scale Mul 1.458 | Background 0.014,1.000 | Import

00-046-1045 (*) - Quartz, syn - SiO_2 - Y: 68.14 % - d x by: 1. - WL: 1.5406 - 0 - I/lc PDF 3.4 -

00-046-1045 (*) - Quartz, syn - SiO_2 - Y: 33.87 % - d x by: 1. - WL: 1.54439 - 0 - I/lc PDF 3.4 -

00-019-0932 (I) - Microcline, intermediate - KAlSi_3O_8 - Y: 12.51 % - d x by: 1. - WL: 1.5406 - 0 -

00-009-0466 (*) - Albite, ordered - $\text{NaAlSi}_3\text{O}_8$ - Y: 8.34 % - d x by: 1. - WL: 1.5406 - 0 - I/lc PDF 2.1 -

01-082-2450 (C) - Muscovite - $(\text{Na}_0.07\text{K}_0.90\text{Ba}_0.01)(\text{Al}_1.84\text{Ti}_0.04\text{Fe}_0.07\text{Mg}_0.04)(\text{Si}_3.02\text{Al}_0.98)\text{O}_{10}$ - Y: 0.44

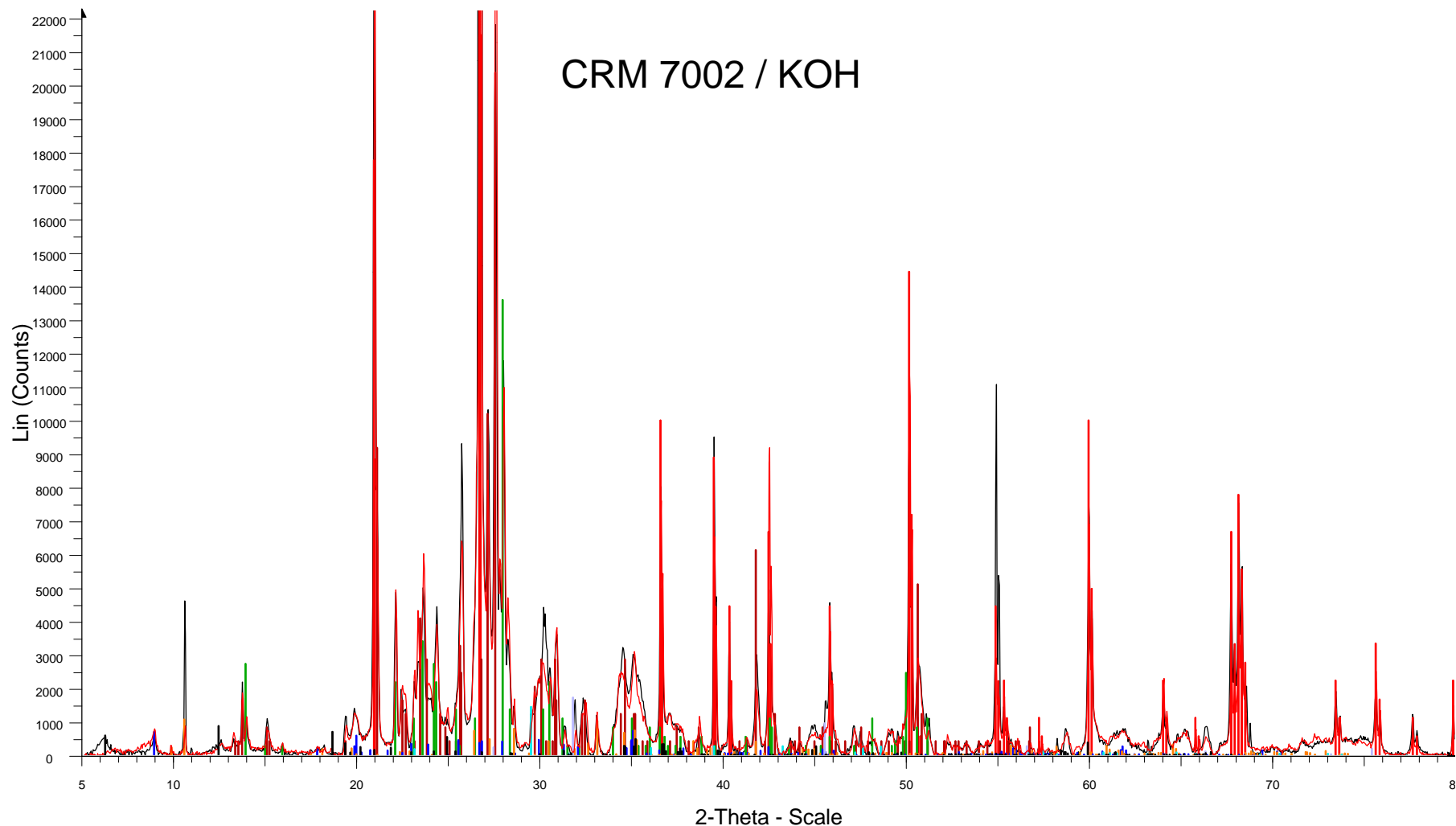
01-082-0038 (C) - Clinocllore Ilb-4 (Cr-, Mg-rich) - $(\text{Mg}_{0.99}\text{Al}_0.01)_5(\text{Al}_0.67\text{Fe}_0.33)(\text{Si}_3.02\text{Al}_0.98)\text{O}_{10}(\text{OH})_8$ - Y:

01-071-1060 (C) - Hornblende - $\text{Na}_9\text{K}_4\text{Ca}_{1.6}\text{Mg}_{2.9}\text{Fe}_{1.4}\text{Ti}_5\text{Al}_2.4\text{Si}_6\text{O}_{24}$ - Y: 0.65 % - d x by: 1. - WL: 1.5406

00-005-0586 (*) - Calcite, syn - CaCO_3 - Y: 0.88 % - d x by: 1. - WL: 1.5406 - Rhombo.H.axes - a 4.98276 - b 4.

00-005-0628 (*) - Halite, syn - NaCl - Y: 1.05 % - d x by: 1. - WL: 1.5406 - Cubic - a 5.63080 - b 5.63080 - c 5.63

Fig. E2c. Normalized X-ray diffraction patterns of CRM 7002 before and after KOH extraction (black and red traces, respectively) showing identified minerals (colored ticks)



Batch3 - CRM 7002 non attaqué - File: BT3_SylSteph.RAW - Type: 2Th/Th locked - Start: 5.000 ° - End: 80.000
Operations: Background 0.120,1.000 | Import

Sample F batch1 - File: BT12_SylSteph.RAW - Type: 2Th/Th locked - Start: 5.000 ° - End: 80.000 ° - Step: 0.04
Operations: Y Scale Mul 1.125 | Background 0.014,1.000 | Import

00-046-1045 (*) - Quartz, syn - SiO₂ - Y: 68.14 % - d x by: 1. - WL: 1.5406 - 0 - I/lc PDF 3.4 -

00-046-1045 (*) - Quartz, syn - SiO₂ - Y: 33.87 % - d x by: 1. - WL: 1.54439 - 0 - I/lc PDF 3.4 -

00-019-0932 (I) - Microcline, intermediate - KAlSi₃O₈ - Y: 12.51 % - d x by: 1. - WL: 1.5406 - 0 -

00-009-0466 (*) - Albite, ordered - NaAlSi₃O₈ - Y: 8.34 % - d x by: 1. - WL: 1.5406 - 0 - I/lc PDF 2.1 -

01-082-2450 (C) - Muscovite - (Na_{0.07}K_{0.90}Ba_{0.01})(Al_{1.84}Ti_{0.04}Fe_{0.07}Mg_{0.04})(Si_{3.02}Al_{0.98})O₁₀(- Y: 0.44

01-082-0038 (C) - Clinocllore Ilb-4 (Cr-, Mg-rich) - (Mg_{0.99}Al_{0.01})₅(Al_{0.67}Fe_{0.33})(Si_{3.02}Al_{0.98})O₁₀(OH)₈ - Y:

01-071-1060 (C) - Hornblende - Na₉K₄Ca_{1.6}Mg_{2.9}Fe_{1.4}Ti₅Al_{2.4}Si₆O₂₄ - Y: 0.65 % - d x by: 1. - WL: 1.5406

00-005-0586 (*) - Calcite, syn - CaCO₃ - Y: 0.88 % - d x by: 1. - WL: 1.5406 - Rhombo.H.axes - a 4.98276 - b 4.

00-005-0628 (*) - Halite, syn - NaCl - Y: 1.05 % - d x by: 1. - WL: 1.5406 - Cubic - a 5.63080 - b 5.63080 - c 5.63

Fig. E2d. Normalized X-ray diffraction patterns of CRM 7002 before and after ascorbate extraction (black and red traces, respectively) showing identified minerals (colored ticks)

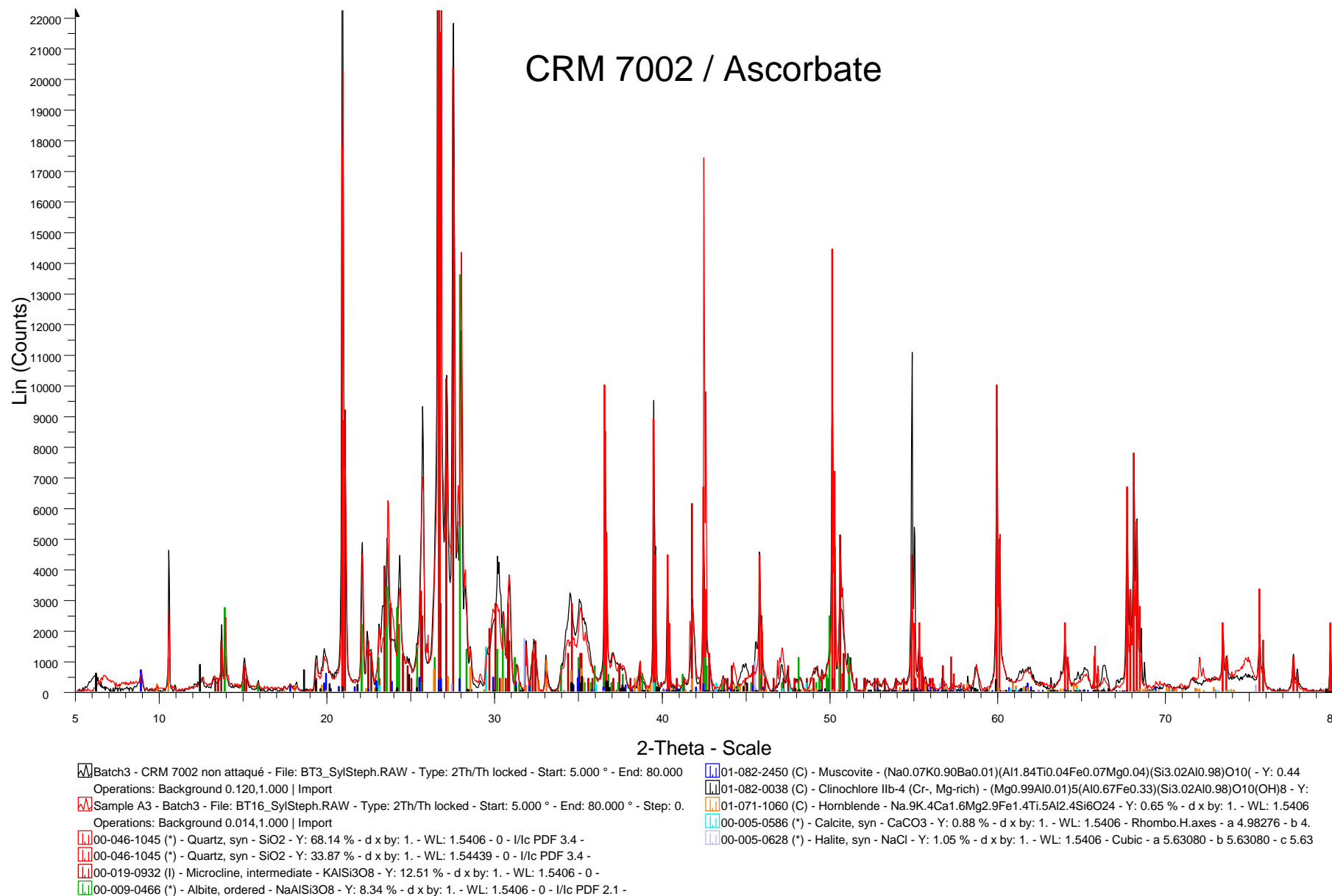


Fig. E2e. Normalized X-ray diffraction patterns of CRM 7002 before and after HCl extraction (black and red traces, respectively) showing identified minerals (colored ticks)

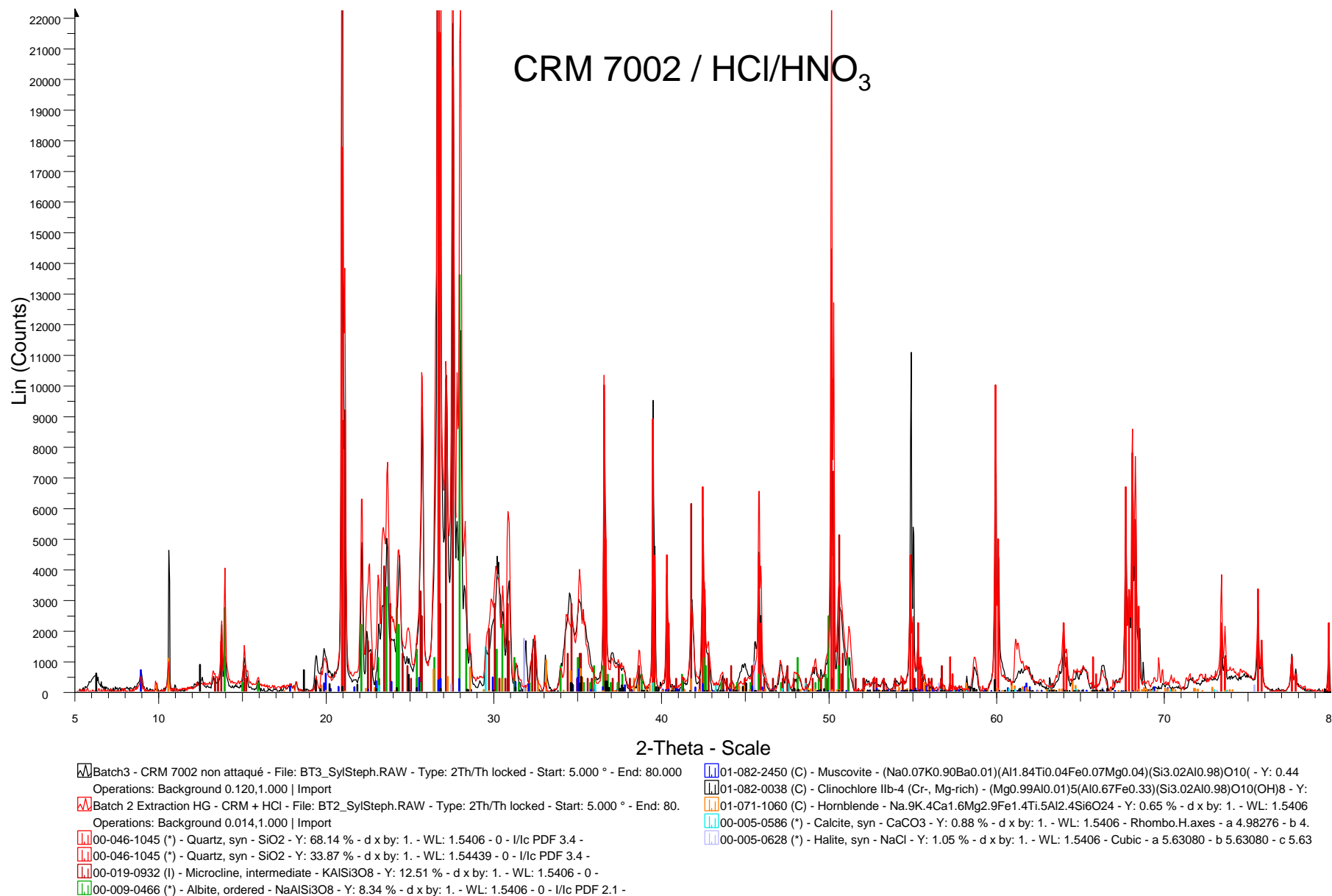
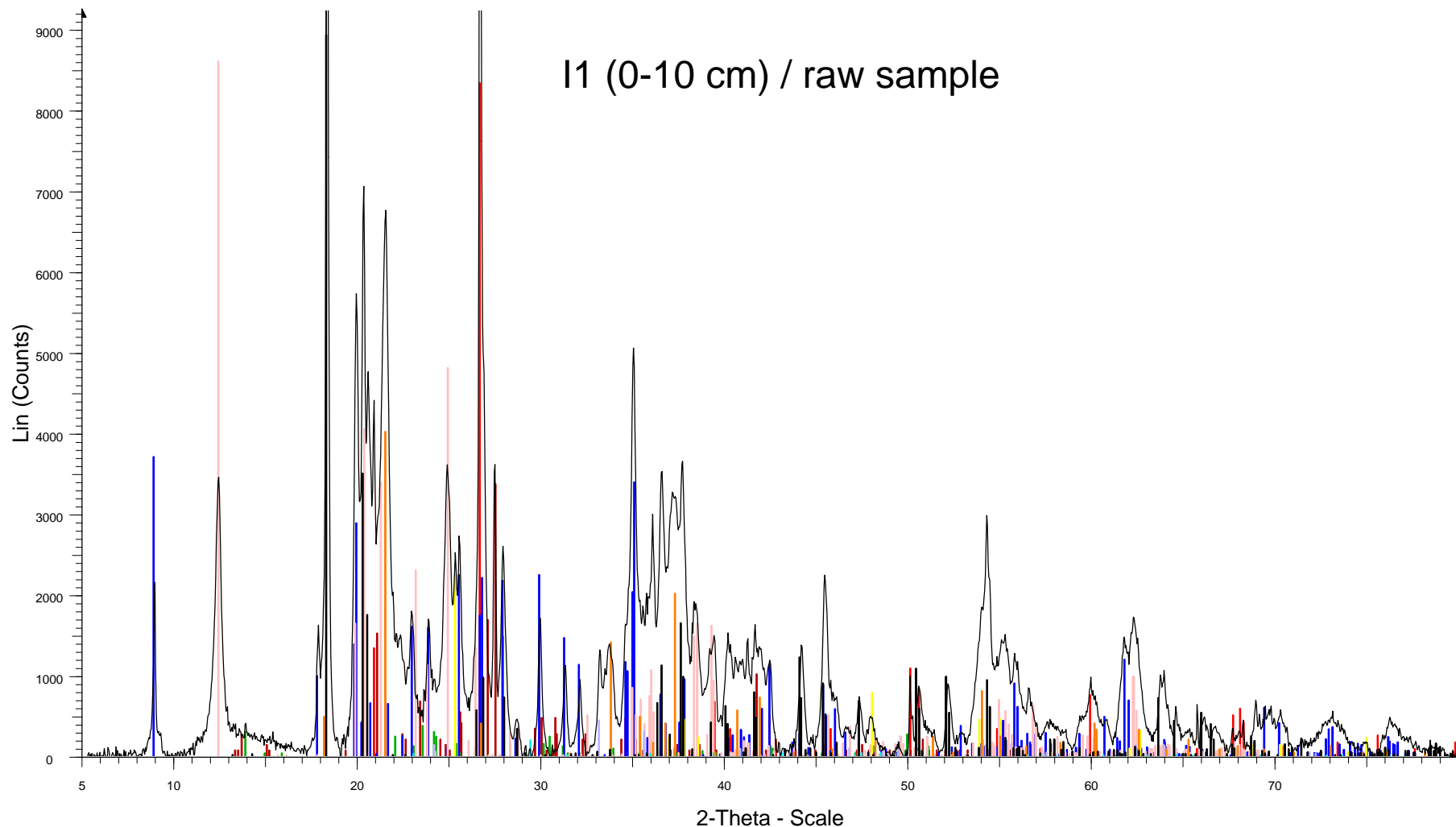


Fig. E3a. X-ray diffraction pattern of sample I-1(0-10m) (black trace) showing identified minerals (colored ticks)

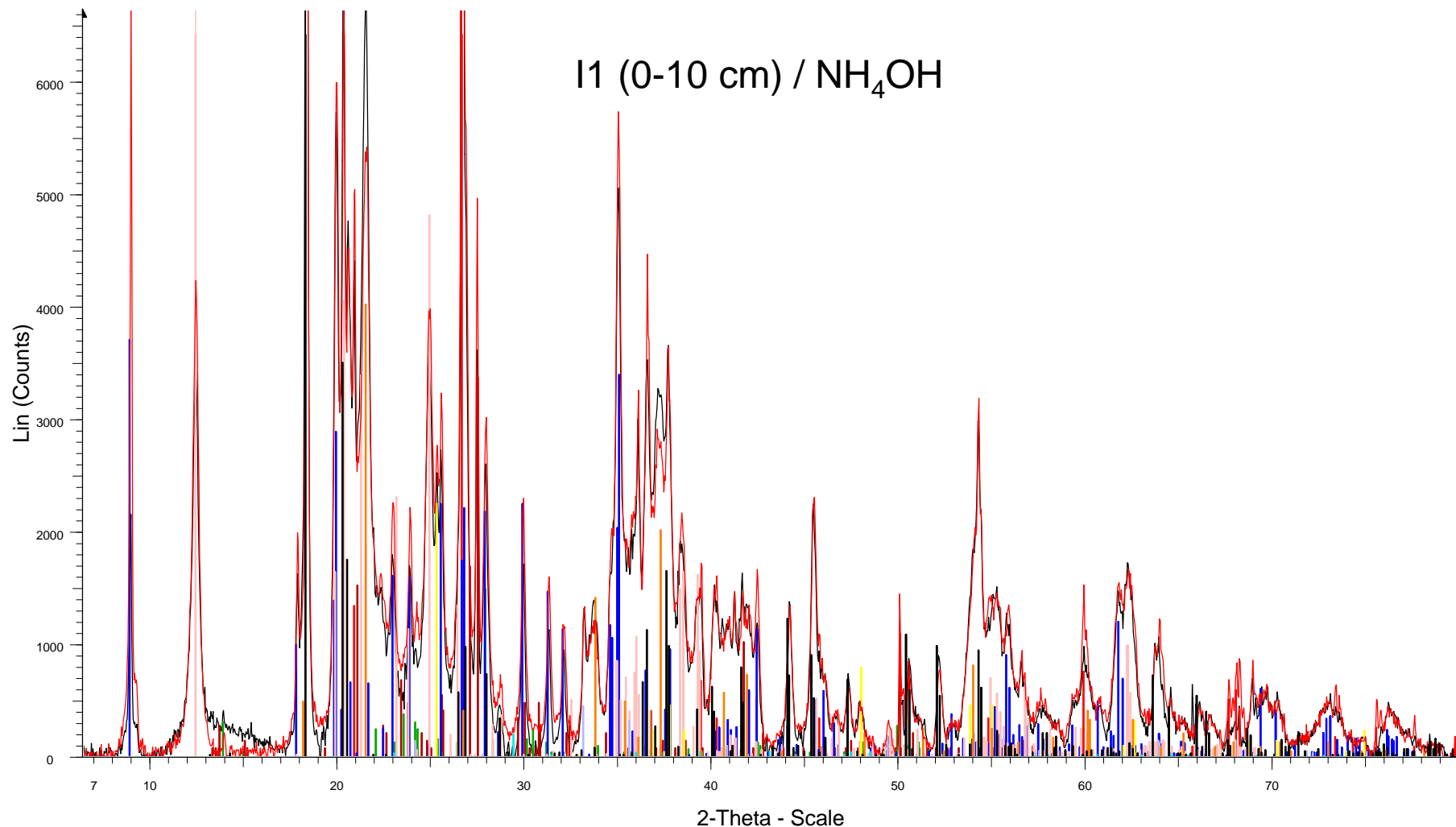


Batch 7 -- M1 sans attaque - File: BT7_SylSteph_bl.RAW - Type: 2Th/Th locked - Start: 5.000 ° - End: 80.000 °
Operations: Background 0.014,1.000 | Import

00-046-1045 (*) - Quartz, syn - SiO₂ - Y: 57.51 % - d x by: 1. - WL: 1.5406 - Hexagonal - a 4.91344 - b 4.91344
00-019-0932 (I) - Microcline, intermediate - KAlSi₃O₈ - Y: 23.23 % - d x by: 1. - WL: 1.5406 - Triclinic - a 8.560 - b 8.560
00-009-0466 (*) - Albite, ordered - NaAlSi₃O₈ - Y: 10.22 % - d x by: 1. - WL: 1.5406 - Triclinic - a 8.144 - b 12.7
01-080-0742 (C) - Muscovite 2M1 - (K_{0.82}Na_{0.18})(Fe_{0.03}Al_{1.97})(AlSi₃)O₁₀(OH)₂ - Y: 25.54 % - d x by: 1. - WL: 1.5406 - Triclinic - a 5.15770 - b 8.15770
01-080-0886 (C) - Kaolinite - Al₂(Si₂O₅)(OH)₄ - Y: 59.38 % - d x by: 1. - WL: 1.5406 - Triclinic - a 5.15770 - b 8.15770
00-005-0586 (*) - Calcite, syn - CaCO₃ - Y: 1.31 % - d x by: 1. - WL: 1.5406 - Rhombo.H.axes - a 4.989 - b 4.98

00-021-1272 (*) - Anatase, syn - TiO₂ - Y: 15.48 % - d x by: 1. - WL: 1.5406 - Tetragonal - a 3.7852 - b 3.78520
01-070-2038 (C) - Gibbsite - Al(OH)₃ - Y: 69.49 % - d x by: 1. - WL: 1.5406 - Monoclinic - a 8.68400 - b 5.07800
00-033-0664 (*) - Hematite, syn - Fe₂O₃ - Y: 3.03 % - d x by: 1. - WL: 1.5406 - Rhombo.H.axes - a 5.0356 - b 5.0356
00-029-0713 (I) - Goethite - Fe₃O(OH) - Y: 27.70 % - d x by: 1. - WL: 1.5406 - Orthorhombic - a 4.56000 - b 9.56000

Fig. E3b. Normalized X-ray diffraction patterns of sample I-1(0-10m) before and after NH_4OH extraction (black and red traces, respectively) showing identified minerals (colored ticks)



[Batch 7 -- M1 sans attaque - File: BT7_SylSteph_bl.RAW - Type: 2Th/Th locked - Start: 5.000 ° - End: 80.000 °
 Operations: Background 0.014,1.000 | Import
 [N1-batch1 - File: BT25_BL.RAW - Type: 2Th/Th locked - Start: 5.000 ° - End: 80.000 ° - Step: 0.040 ° - Step tim
 Operations: Y Scale Mul 1.000 | Y Scale Mul 1.500 | Background 0.000,1.000 | Import
 [00-046-1045 (*) - Quartz, syn - SiO_2 - Y: 42.31 % - d x by: 1. - WL: 1.5406 - Hexagonal - a 4.91344 - b 4.91344
 [00-019-0932 (I) - Microcline, intermediate - KAlSi_3O_8 - Y: 17.09 % - d x by: 1. - WL: 1.5406 - Triclinic - a 8.560 -
 [00-009-0466 (*) - Albite, ordered - $\text{NaAlSi}_3\text{O}_8$ - Y: 7.52 % - d x by: 1. - WL: 1.5406 - Triclinic - a 8.144 - b 12.78
 [01-080-0742 (C) - Muscovite 2M1 - $(\text{K}_{0.82}\text{Na}_{0.18})(\text{Fe}_{0.03}\text{Al}_{1.97})(\text{AlSi}_3\text{O}_{10})(\text{OH})_2$ - Y: 18.79 % - d x by: 1. - WL: 1.5406 - Triclinic - a 5.15770 - b 8.
 [01-080-0886 (C) - Kaolinite - $\text{Al}_2(\text{Si}_2\text{O}_5)(\text{OH})_4$ - Y: 43.69 % - d x by: 1. - WL: 1.5406 - Triclinic - a 5.15770 - b 8.
 [00-005-0586 (*) - Calcite, syn - CaCO_3 - Y: 0.97 % - d x by: 1. - WL: 1.5406 - Rhombo.H.axes - a 4.989 - b 4.98
 [00-021-1272 (*) - Anatase, syn - TiO_2 - Y: 11.39 % - d x by: 1. - WL: 1.5406 - Tetragonal - a 3.7852 - b 3.78520
 [01-070-2038 (C) - Gibbsite - $\text{Al}(\text{OH})_3$ - Y: 51.13 % - d x by: 1. - WL: 1.5406 - Monoclinic - a 8.68400 - b 5.07800
 [00-033-0664 (*) - Hematite, syn - Fe_2O_3 - Y: 2.23 % - d x by: 1. - WL: 1.5406 - Rhombo.H.axes - a 5.0356 - b 5.
 [00-029-0713 (I) - Goethite - $\text{Fe}+3\text{O}(\text{OH})$ - Y: 20.38 % - d x by: 1. - WL: 1.5406 - Orthorhombic - a 4.56000 - b 9.

Fig. E3c. Normalized X-ray diffraction patterns of sample I-1(0-10m) before and after KOH extraction (black and red traces, respectively) showing identified minerals (colored ticks)

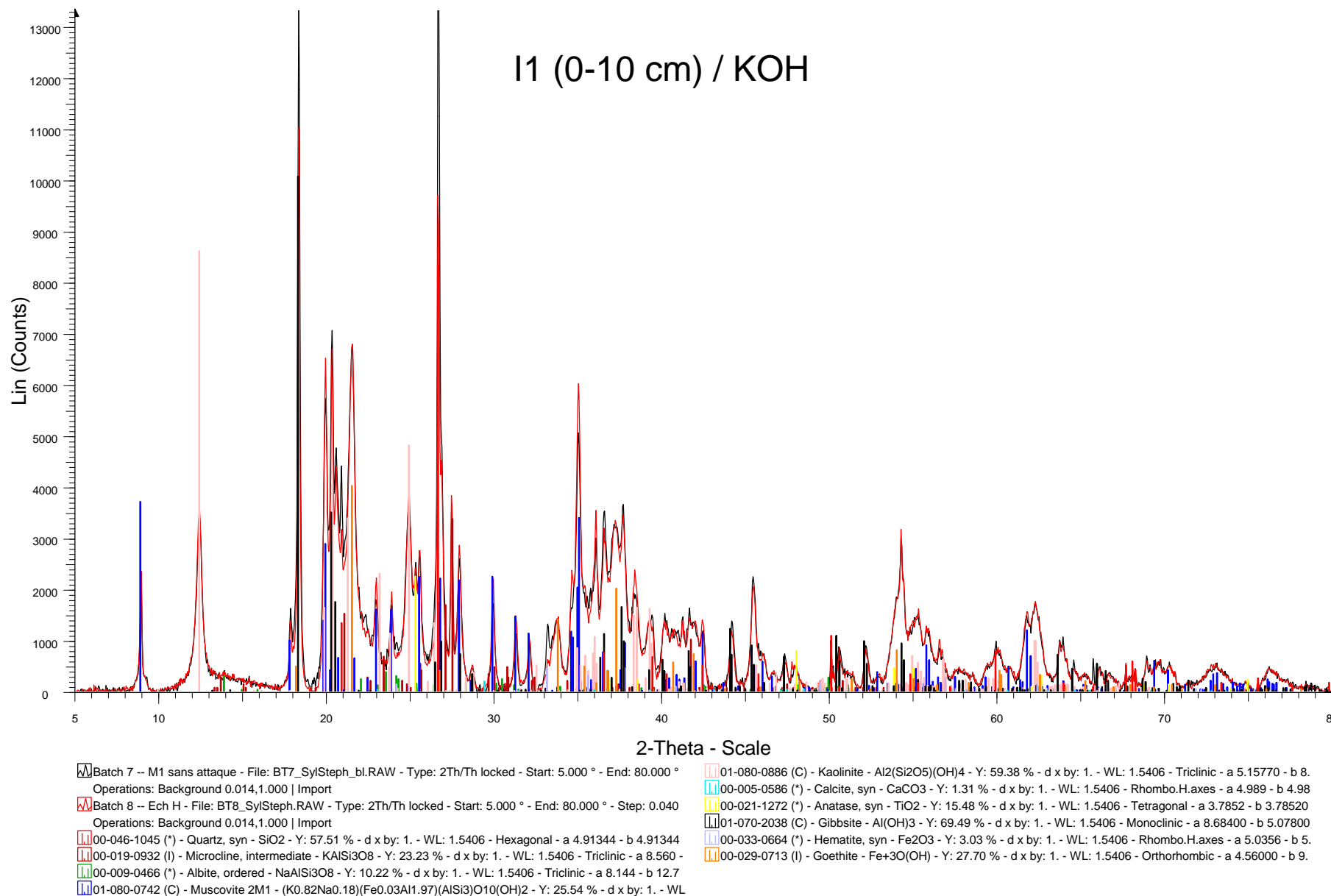


Fig. E3d. Normalized X-ray diffraction patterns of sample I-1(0-10m) before and after ascorbate extraction (black and red traces, respectively) showing identified minerals (colored ticks)

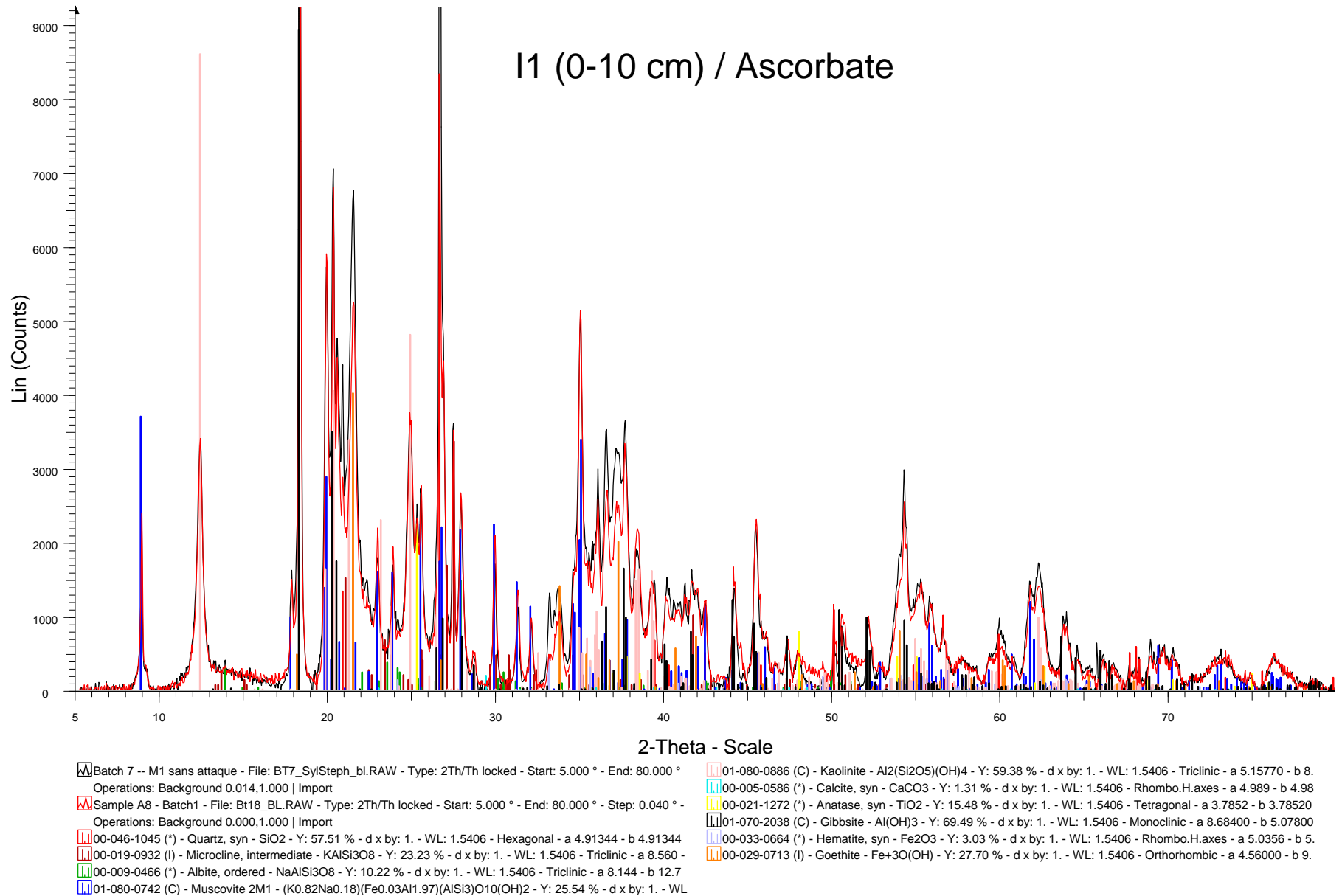


Fig. E3e. Normalized X-ray diffraction patterns of sample I-1(0-10m) before and after HCl extraction (black and red traces, respectively) showing identified minerals (colored ticks)

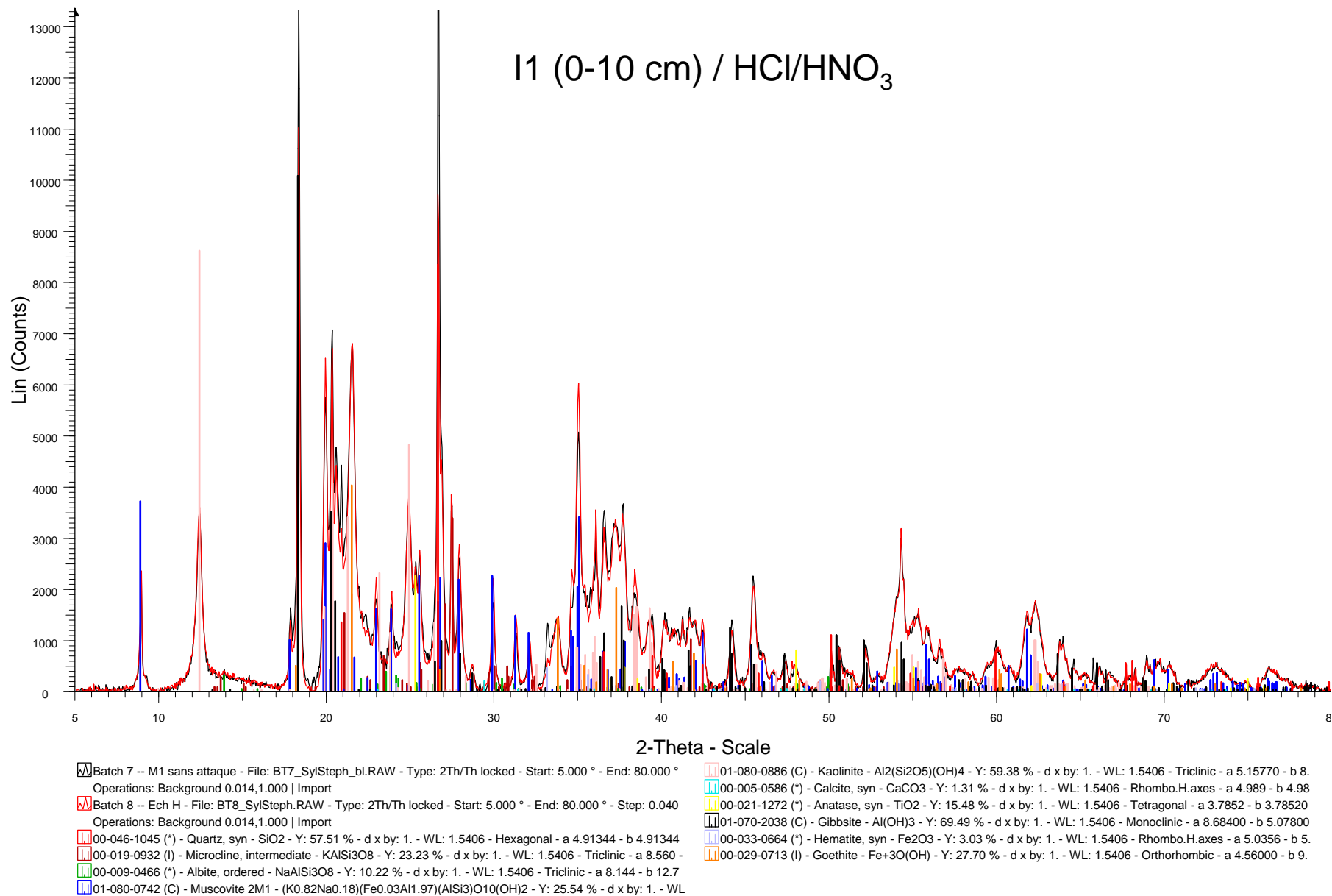
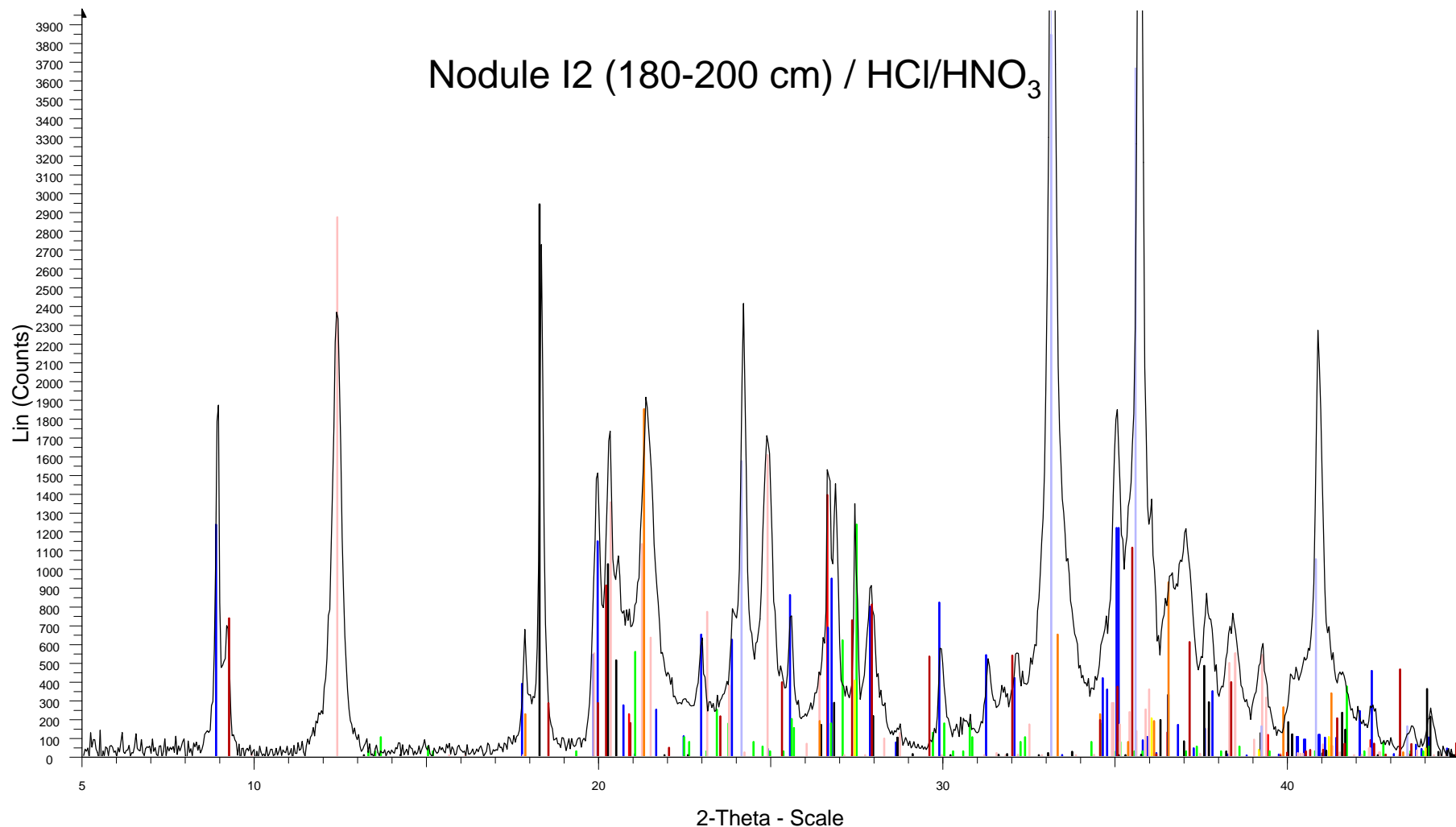


Fig. E4. X-ray diffraction pattern of nodules from sample I-1(180-200m) (black trace) showing identified minerals (colored ticks)



M1 180-200 Batch1 - File: BT34_SylSteph_uni.RAW - Type: 2Th/Th locked - Start: 5.000 ° - End: 80.000 ° - Ste
Operations: Background 0.000,0.000 | Import

00-046-1045 (*) - Quartz, syn - SiO₂ - Y: 23.52 % - d x by: 1. - WL: 1.5406 - Hexagonal - a 4.91344 - b 4.91344

01-086-1384 (C) - Muscovite 2M1 - K_{0.894}Al_{1.93}(Al_{0.943}Si_{2.829}O₁₀)(OH)_{1.744}F_{0.256} - Y: 20.84 % - d x by:

01-083-2129 (C) - Paragonite 3T - NaAl₂(Si₃Al)O₁₀(OH)₂ - Y: 18.76 % - d x by: 1. - WL: 1.5406 - Hexagonal - a

00-019-0932 (I) - Microcline, intermediate - KAlSi₃O₈ - Y: 20.84 % - d x by: 1. - WL: 1.5406 - Triclinic - a 8.560 -

01-080-0886 (C) - Kaolinite - Al₂(Si₂O₅)(OH)₄ - Y: 48.56 % - d x by: 1. - WL: 1.5406 - Triclinic - a 5.15770 - b 8.

01-070-2038 (C) - Gibbsite - Al(OH)₃ - Y: 49.73 % - d x by: 1. - WL: 1.5406 - Monoclinic - a 8.68400 - b 5.07800

00-033-0664 (*) - Hematite, syn - Fe₂O₃ - Y: 88.55 % - d x by: 1. - WL: 1.5406 - Rhombo.H.axes - a 5.0356 - b

00-029-0713 (I) - Goethite - Fe₂O₃(OH) - Y: 31.26 % - d x by: 1. - WL: 1.5406 - Orthorhombic - a 4.59072 - b 9.

00-021-1276 (*) - Rutile, syn - TiO₂ - Y: 6.78 % - d x by: 1. - WL: 1.5406 - Tetragonal - a 4.5933 - b 4.59330 - c

Fig. E5.

